The *Drosophila* Circadian Clock Gene *Cycle* Controls Development of Clock Neurons

Grace Biondi[1], Gina McCormick[1] and Maria P. Fernandez[1,2]

1- Department of Neuroscience and Behavior, Barnard College. New York, NY 10027
2- Corresponding author mfernand@barnard.edu

Abstract

Daily behavioral and physiological rhythms are controlled by the brain's circadian timekeeping system, a synchronized network of neurons that maintains endogenous molecular oscillations. These oscillations are based on transcriptional feedback loops of clock genes, which in *Drosophila* include the transcriptional activators *Clock (Clk)* and *cycle (cyc)*. While the mechanisms underlying this molecular clock are very well characterized, the roles that the core clock genes play in neuronal physiology and development are much less understood. The *Drosophila* timekeeping center is composed of ~150 clock neurons, among which the four small ventral lateral neurons (sLN_vs) are the most dominant pacemakers under constant conditions. The sLN_vs express the neuropeptide Pigment Dispersing Factor (PDF), a key output signal within the clock neuron network. Here, we show that downregulating the clock gene *cyc* specifically in the *Pdf*-expressing neurons prevents the formation of axonal bundles within which projections normally navigate toward the dorsal brain. This effect is due to a developmental role of *cyc*, as both knockdown *cyc* or expressing a dominant negative form of *cyc* exclusively during development lead to phenotypes in adult clock neurons. Expressing a dominant negative *Clk* also leads to developmental effects on sLNv morphology, but *cyc* and *clk* manipulations produce distinct phenotypes. Our results reveal a non-circadian role for *cyc*, shedding light on additional functions of circadian clock genes in the development of the nervous system.

Keywords: neuronal development, fasciculation, circadian clock, cycle, *Drosophila*

Introduction

The proper wiring of neuronal circuits during development is essential for neuronal control of behavior. Across animal species, rhythms in sleep/wake cycles as well as many other behavioral and physiological rhythms are controlled by the circadian timekeeping system, a network of neurons that is capable of maintaining endogenous molecular oscillations with a ~24 period [1]. Proper functioning of the circadian neuron network requires the formation of the synaptic and peptidergic connections during development [2, 3].

The *Drosophila* circadian clock neuron network (CCNN), the functional equivalent of the mammalian suprachiasmatic nuclei, consists of ~150 neurons [4-6]. All neurons in the CCNN contain an intracellular molecular clock based on a transcriptional feedback loop of clock genes [7]. CLOCK (CLK) and CYCLE (CYC) are heterodimeric transcriptional activators and initiate the function of this feedback loop by promoting the expression of the repressors PERIOD (PER) and TIMELESS (TIM) [8]. PER-TIM inhibit CLK-CYC function until they are degraded, which enables the cycle to reinitiate every morning. CLK/CYC also interact with other genes in a secondary circadian loop by activating the genes *vrille* (*vri*), and *par domain protein*ε (*pdp1*ε) [9, 10]. *Clk* and *cyc* expression can be detected in almost all clock neurons even before some of those clock groups show *per* molecular oscillations [11], suggesting they serve functions the precede the establishment of molecular circadian rhythms.

Cyc is a homolog of the mammalian *bmal1*, although unlike BMAL1 and the other *Drosophila* circadian proteins, CYC protein levels do not cycle [12]. There is growing evidence for noncircadian functions of *bmal1*: BMAL1 downregulation induces apoptosis and cell-cycle arrest in Glioblastoma Stem Cells (GSC) and was found to preferentially bind metabolic genes and associate with active chromatin regions in GSCs [13]. A CRISPR/Cas9 brain knockdown of *bmal1* caused glioblastomas to grow at faster rates compared to controls [14], and similar effects were observed in B16 melanoma cells [14]. Moreover, *Bmal1*(-/-) mice have defects in defects in short- and long-term memory formation [15] and show reduced lifespan and multiple symptoms of premature aging [16]. Results from studies in different animal models suggest that *Bmal1* may play a role in the development of various neurological disorders [17].

Neurons in the CCNN can be classified into multiple clusters with distinct patterns of gene expression, anatomy, physiology, and synaptic connectivity [5, 6, 18-24]. Among them, the small ventral lateral neurons (sLN_vs) are considered the most dominant pacemaker since they are critical for maintaining behavioral rhythmicity under constant darkness and temperature (DD, or free-running) [25-28]. The sLN_vs, along with the large LN_vs, release the neuropeptide Pigment Dispersing Factor (PDF) [29], which is required to maintain synchrony within the clock neuron network [30]. PDF accumulates rhythmically at the sLN_v dorsal termini [31] and can be released from both the neurites and soma [32]. The loss of PDF severely reduces the amplitude the endogenous circadian rhythm and produces a shortening of its free-running period under DD [29]. The lLN_vs do not play a role in maintaining rhythms under free running [25], but mediate arousal [33].

The projections of the four sLN_vs extend forming a bundle as they navigate from the ventral to the dorsal brain. These projections are usually difficult to separate from each other until they begin to defasciculate [34], extending their dorsal arborizations towards the area where dorsal clusters of circadian clock neurons are located [35]. In adult flies, the sLN_v dorsal termini undergo clock-controlled structural plasticity in their dorsal projections [36], a rhythm that relies on daily and circadian rhythms in the outgrowth and de-fasciculation of terminal arborizations [37-40].

Both *Clk* and *cyc* null mutations lead to a severe reduction *pdf* RNA, and the PDF signal can barely be detected in the sLNv projections [31, 41]. We downregulated *cyc* specifically in the *Pdf*$^+$ cells and observed a pronounced defasciculation of the sLN_v projections, which no longer navigate towards the dorsal brain forming bundles. Similar phenotypes were observed by expressing a dominant negative form of *cyc* [42]. Moreover, *cyc* downregulation in *Pdf*+ cells during development is sufficient to prevent the fasciculation of the adult sLN_vs and results in the loss of behavioral rhythms. Manipulations of *Clk* expression also affect sLNv morphology, but the phenotypes are different from those resulting from *cyc* manipulations. Our results show that *cyc* plays a role in the development of pacemaker neurons, which is likely independent from its role in the circadian molecular oscillator.

Results

Cyc downregulation in circadian pacemaker neurons prevents the formation of sLN_vs axon bundles

Mutations in both *Clk* and *cyc* severely reduce *pdf* RNA and neuropeptide levels [31, 41]. In *cyc* null mutants, the projections of the sLN_vs cannot be detected in larvae or adult brains when staining with PDF antibodies [31, 43, 44]. We observed that at ZT2, *cyc* null mutants (cyc^{01}) showed a substantial reduction in PDF levels compared to Canton-S controls, consistent with previous studies (Fig 1A). However, upon examination at higher magnification and intensity we noticed the presence of thin, misrouted sLN_vs projections in cyc^{01} flies (Fig 1A, right panels). Upon close observation, PDF could often be detected in the sLN_v projections, including the dorsal termini. These projections do not form the stereotypical bundle seen in control brains when extending from the anterior medulla towards the dorsal area of the brain.

Since highly defasciculated projections might contribute to the weaker PDF levels observed in cyc^{01} mutants, we examined the structure of the sLN_v projections using a *Pdf*-RFP transgene in which a cytosolic Red Fluorescent Protein (RFP) was placed under the control of the *Pdf* regulatory sequence[45]. As expected, the projections from the four sLN_v projections remain fasciculated, forming a bundle, until they reach the superior medial protocerebrum (SMP) in control brains. In contrast, the sLN_vs of cyc^{01} mutants they often begin to defasciculate in the ventral brain near the cell bodies (Fig 1B). Some sLN_v projections are severely misrouted and do not reach the dorsal brain, extending towards the midline or other brain regions, while projections that do reach this area appear thin and are rarely fasciculated. As a result, it is possible to distinguish individual projections from each of the four sLN_vs in the cyc^{01} mutant, something that it is not possible in the controls until the projections reach the main branching point in the superior medial protocerebrum.

Next, we drove expression of a *cyc* dsRNA (cyc^{RNAi}) under the control of a *Pdf*-Gal driver to determine if the effect of *cyc* loss on the sLN_vs is cell-autonomous. Starting at the point where the projections of the sLN_v intersect with those of the lLNvs ('point of origin', POI, Fig. S1A), we quantified the length until the first branching point ('branching point', BP, Fig. S1A). In the control brains, the branching point is the place where the sLN_vs ramify and extend their stereotypical arborizations in the dorsal protocerebrum. These arborizations show daily, clock-controlled

rhythms in their fasciculation and outgrowth [36]. Downregulation of *cyc* in the *Pdf*-expressing cells via cyc^{RNAi} resulted in a significantly shorter distances to branching points (Fig 1C). This phenotype resembles a milder version of the cyc^{01} phenotype, since defasciculation appears shortly after the projections begin to extend from the cell bodies. Using a modified Scholl's analysis [46], we quantified the degree of branching in the projections starting at the POI and observed pronounced defasciculation throughout the projection of cyc^{01} sLN_vs (Fig 1D). The total projection length was not different from the controls (Fig 1E). The defasciculation phenotype was not observed in the contralateral projections that extend from the lLN_vs (Fig 1F). Since the lLN_vs are born later in development, during metamorphosis [34], this suggests that *cyc* might play a role in neuronal development during an earlier developmental stage, when the sLN_vs begin to extend their projections towards the dorsal brain.

Expression of dominant negative forms of *Clk* and *cyc* is an effective strategy to prevent circadian molecular oscillations in different clock neuron groups [42, 47, 48]. Based on the phenotypes induced by *cyc* downregulation, we asked if expressing a dominant negative form of *cyc* in the sLN_vs would also lead to aberrant projection morphology. We found that when we drove expression of Δ-*cyc* using *Pdf*-Gal4, the sLN_vs had a significantly shorter distance until branching point (Fig S2A-B) and a higher degree of sLN_v projection defasciculation (Fig S2A,C), similar to the effects observed in *Pdf>* cyc^{RNAi} sLN_vs. The total projection length was not affected (Fig. S2D), nor were the projections of the lLN_vs (Fig. S2E).

PER levels in *Pdf*+ neurons are reduced upon cell-specific *cyc* knockdown

Cyc activates *per* transcription, and therefore PER levels in the brain are therefore significantly reduced in *cyc* mutants [12]. To confirm that the phenotypes of cyc^{RNAi} expression in the *Pdf*-expressing neurons are consistent with what is expected from a cell-specific reduction in *cyc* levels, we stained brains from heterozygote parental controls (;uas-cyc^{RNAi}/+; and *Pdf-Gal4,Pdf-DsRed/+;*) and *Pdf>*cyc^{RNAi} flies at the end of the night (ZT23), when PER nuclear levels are highest [49]. We found that *Pdf>*cyc^{RNAi} flies showed significantly lower nuclear PER levels in both the sLN_vs (Fig 2A-B) and the lLN_vs (Fig 2C-D). In contrast, in the Lateral Neurons Dorsal

(LN_ds), PER expression levels were not affected (Fig 2E-F). This confirms that at least under LD, the *Pdf>cyc*^{RNAi} manipulation results in a reduction in PER expression only in *Pdf*$^{+}$ clock neurons.

A null *cyc* mutation leads to pronounced behavioral phenotypes: during a light dark cycle (LD), activity is unimodal instead of bimodal, and flies are largely nocturnal [50]. Under free-running conditions, *cyc* mutants are largely arrhythmic due to the key role that *cyc* plays in sustaining molecular oscillations [12]. We conducted behavioral experiments to determine the extent to which downregulating *cyc* specifically in PDF-expressing neurons recapitulates the phenotype of the *cyc* mutant. Under LD, the activity pattern of *Pdf>cyc*^{RNAi} flies is bimodal and they do not show the pronounced nocturnality characteristic of the *cyc* mutant (Fig 2G), indicating that these phenotypes in the mutant are due to the loss of the gene in non-*Pdf*+ cells. However, under free-running conditions, the majority (93.75%) of the experimental flies are arrhythmic, supporting the notion that the *cyc*^{RNAi} line is effectively reducing *cyc* levels in the sLN_vs (Fig 2H).

Cyc acts during development to shape neuronal morphology in adults

Cyc downregulation results in the defasciculation of the sLN_v projections starting in the ventral brain, in proximity to the cell bodies (Fig 1A). The sLN_vs begin to extend their projections towards the dorsoposterior brain during the larval stages, suggesting that *cyc* exerts a developmental effect [51]. To knockdown *cyc* specifically during development we employed a temperature-sensitive Gal80 variant with ubiquitous expression to conditionally inhibit Gal4 mediated expression of *cyc*^{RNAi} [52]. This enables temporal regulation of UAS transgenes, as Gal80^{ts} remains active at lower temperatures but becomes inactive at higher temperatures. We raised flies at 28˚C to prevent expression of *cyc*^{RNAi} and transferred them to 18˚C immediately after eclosion (see methods section). After one week at 18˚C, brains were dissected at ZT2 and stained with PDF and RFP antibodies.

Results shown in Figure 3 indicate that downregulating *cyc* only exclusively before eclosion results in abnormal morphology of the sLN_v axonal projections in adult flies (Fig 3A). The phenotypes resemble those seen with constitutive downregulation; significantly shorter distance to the first branching point (Fig 3A-B) and a higher degree of defasciculation compared to parental controls

(Fig 3A,C). No significant differences were found in the total projection length or the degree of defasciculation of the lLN_vs, (Fig 3D-E). To determine if adult-specific *cyc* knockdown in the *Pdf*-expressing would also lead to morphological phenotypes cells, we raised flies at the restrictive temperature (18˚C) and switched them to the permissive temperature (28˚C) immediately after eclosion (see methods section). This manipulation did not result in morphology phenotypes either in length to the branching point or degree of sLN_v defasciculation (Fig. S3A-E). Taken together, these results suggest that *cyc* plays a role in sLN_v fasciculation during development.

A previous study showed that panneuronal rescue of *cyc* expression in a cyc^{01} mutant exclusively during development was sufficient to partially rescue arrhythmicity in adult flies [44]. We wondered if downregulating *cyc* in the *Pdf*+ cells specifically during development would also lead to behavioral phenotypes similar to those seen in the *cyc* null mutants. Using the same protocol described above, we raised control and experimental flies at restrictive temperature and switched them to permissive temperature upon eclosion. Under free-running conditions, most (~78%) $Pdf>cyc^{RNAi}$ flies are arrhythmic (Fig. S3F-H). This indicates that developmental knockdown of *cyc* specifically in the *Pdf*+ cells is sufficient to prevent behavioral rhythms in adults.

Cyc manipulations lead to aberrant sLN_v projections in larval clock neurons

In the experiments described above, *cyc* expression was downregulated throughout development until the end of metamorphosis. To determine if *cyc* plays a role in shaping the morphology of clock neurons during earlier developmental stages, we performed the same experiments as above in the third larval instar (L3) (Fig 4). Length until branching point was not different from controls (4A-B), but there was a significantly higher degree of sLN_v branching (4A-C). This quantification is similar to the one previously described to quantify arborization of the sLN_vs dorsal projections in adults [36], where the concentric circles are centered in the main branching point (Fig. S1B, see methods section). The total sLN_v projection length was not affected (Fig 4D).

Since in adults the effects of *cyc* knockdown via RNAi and expressing a *cyc* dominant negative in larvae were similar to the effects observed in adults (Fig 1 and Fig S2), we then analyzed the morphology of the sLN_v projections in *Pdf*>-Δ-*cyc* L3 larvae. In *Pdf*>-Δ-*cyc* brains the length to

the branching point was significantly reduced (Fig 4E-F) and the number of sLN_v branches was significantly increased compared to controls (Fig 4G). The total sLN_v projection length was not significantly different from that seen in parental controls (Fig 4H). Taken together, these results suggest that *cyc* plays a role in the development of the critical sLN_v pacemaker neurons during the larval stage.

***Clk* and *cyc* have differential effects on neuronal development**

Clk and *cyc* mutations result in similar effects on the expression pattern of PDF in adult brains [31]. CLK and CYC act as a heterodimeric transcriptional activator, and circadian phenotypes described for mutations in these core circadian clock genes, both molecular and behavioral, are also similar [42, 50, 53]. To determine if downregulating *Clk* in the sLN_vs led to the same defasciculation of the sLN_vs we observed with *cyc* manipulations, we performed similar experiments as described above where we expressed Clk^{RNAi} in *Pdf*+ neurons. We found that $Pdf>Clk^{RNAi}$ flies also show neuronal morphology phenotypes (Fig. 5). Consistent with a previous study [54], we detected a very weak and sparse PDF signal along the dorsal sLN_v projections (Fig 5A).

However, RFP labeling of the sLN_v membrane indicates that the dorsal termini are actually more expanded than those of control flies, resulting in significantly higher branching (Fig 5B,E). Unlike $Pdf>cyc^{RNAi}$ flies, neither the distance to the branching point (Fig 5C) nor the degree of defasciculation of the ventral projection was different from controls (Fig 5D). Neither the sLN_v total projection length nor the lLN_v projections were affected (Fig. S4C-D). We conducted behavior experiments and confirmed that Clk^{RNAi} leads to partial loss of free-running rhythms (Fig. S4). Only 50% of the $Pdf>Clk^{RNAi}$ flies were rhythmic, and those that were rhythmic showed a lengthening in free-running period (Fig. S4 A-B, Table 1). Expression of Δ-*Clk* in the *Pdf*+ cells did not result in changes in the sLN_v projection length until branching point (Fig 5F) or degree of defasciculation of the ventral projection (Fig 5G), but led to a significant increase in the total sLN_v projection length (Fig 5H). The length of the lLN_v projections was not affected (Fig. S4E).

We then examined L3 larval brains to determine if the phenotypes were already present at this developmental stage. While expression of *Clk*^{RNAi} did not result in morphology phenotypes in larval LN_vs (Fig. S5), expression of Δ-*Clk* resulted in pronounced phenotypes (Fig 6). We observed a significant increase in sLN_v dorsal termini branching (Fig 6C) and total projection length (Fig 6D) in *Pdf*>-Δ-*cyc* larvae. Length to the branching point for the experimental Δ-*Clk* larvae was not significantly different from control lines (Fig 6B). Expressing the dominant negative *Clk* was more effective than *Clk* downregulation at inducing phenotypes in the larval stage, possibly because the RNAi line is not completely effective at preventing *Clk* expression. These results show that manipulations in *Clk* and *cyc* expression lead to distinct morphological phenotypes in sLN_v axonal bundle formation during development and in extension of the dorsal arborizations.

Discussion

Our results reveal a role for the circadian clock gene *cyc*, shaping the wiring of the key clock pacemaker neurons, the sLN_vs. Constitutive *cyc* knockdown or expression of a dominant negative form of *cyc* in the *Pdf*+ cells result in the inability of the sLN_v to form axonal bundles as they navigate toward the dorsal brain. *Clk* downregulation and expression of a dominant negative form of *Clk* also result in sLN_v morphology phenotypes, although they appear to be distinct from those caused by *cyc* manipulations. Expressing the dominant forms of both *Clk* and *cyc* has been used in previous studies as an effective way to prevent molecular oscillations in subsets of clock neurons. However, our results indicate that those genetic manipulations also lead to additional phenotypes beyond molecular timekeeping that are already detectable during the larval stages.

In addition to the anatomical and functional classifications, clock neurons can be divided into early or late developmental groups depending on when circadian oscillations can be detected. In the early groups, which include the sLN_v, *per* and *tim* expression rhythms can be detected at the first instar (L1) larval stage, whereas in the late groups such rhythms cannot be detected until metamorphosis [34, 55]. However, *cyc* and *clk* expression using GFP-*cyc* and GFP-*Clk* transgenes can be detected in almost all groups of clock neurons in earlier developmental stages, even days before *per* oscillations begin [11]. This suggests that *cyc* and *Clk* might have additional roles in the development of clock neurons beyond their role in the molecular oscillator.

Both *cyc* and *Clk* modulate PDF expression in both larval and adult clock neurons. In *Clk*^{jrk} mutants, neither PDF nor *pdf* mRNA can be detected in larval [41] or adult LN_vs [31], and similar results were obtained in a *cyc* null mutant [31]. A previous study showed that panneuronal rescue of *cyc* expression throughout development is sufficient to restore PDF expression in the LN_v dorsal projections of *cyc*^{01} mutants, and that developmental inhibition of CLK/CYC activity affects PER expression rhythms in the adult LNvs [44]. Moreover, overexpression of *vri*, a clock gene that is downstream of CLK/CYC and acts as a repressor of CLK transcription [10, 41], causes a severe reduction in PDF levels in larval brains [41], and the low PDF levels in the sLN_vs of *cyc*^{01} mutants can be rescued by *vri* expression [43]. However, restoring PDF expression in the sLN_vs in flies that lack *vri* expression is not sufficient to rescue activity rhythms. Manipulations in the levels of PDF or its receptor, PDFR, also result in impaired plasticity rhythms [56] and misrouting of the sLN_v projections [57].

Unlike *cyc* and *Clk* mutants [31], *per*^{01} and *tim*^{01} mutants display PDF expression in the sLN_vs, although its accumulation in the dorsal termini no longer shows oscillations [31]. Structural plasticity rhythms in the sLN_vs are absent in both *per*^{01} and *tim*^{01} mutants [36]. Although the anatomical phenotypes are mild compared to those that we observe when *cyc* and *Clk* are downregulated or when dominant negative forms are expressed, the sLN_v dorsal termini of both *per* and *tim* mutants appear to have altered morphology as well [36]. Downregulation of *Clk* [54] and overexpression of *vri* in *Pdf*-expressing cells [43] also result in impaired plasticity rhythms [56]. It will be interesting to determine the extent to which manipulations of *per/tim* and *vri* expression might also result in developmental phenotypes in clock neurons.

Expression of CLK and CYC is restricted to the CCNN [11], however, *cyc* mRNA is not limited to clock neurons [58]. Expressing *Clk* outside the CCNN can generate ectopic clocks [59], but these ectopic clocks require *cyc*. This suggests that although the CYC protein can only be detected in clock cells, *cyc* mRNA is more broadly expressed, but the protein cannot be detected unless CLK is expressed. A study by Liu et al. showed that *Clk* stabilizes CYC both in cultured *Drosophila* Schneider 2 (S2) cells and *in vivo*: upon *Clk* ectopic expression GFP-CYC can be detected in additional cells beyond the clock neuron network [60]. The role of *cyc* mRNA

expression in non-clock cells remains unknown. Our results suggest that *Clk* and *cyc* may have at least partially distinct roles in shaping the morphology of clock neurons, and it is possible that *cyc* plays a developmental role in non-clock neurons as well.

Materials and Methods

Fly lines and rearing

Flies were raised on cornmeal-sucrose yeast media in a Percival Incubator under 12:12 LD at different temperature conditions. Depending on the experiment flies were raised under either 18˚C or 28˚C (indicated in the figure legend for each experiment). The lines *UAS-cyc*^{RNAi42563}*,UAS-clk*$^{RNAi\ 42566}$, w^{1118} (BDSC #3605) and CS (BDSC #64349) were obtained from the Bloomington *Drosophila* Stock Center. The lines *Pdf-dsRed,Pdf-Gal4;Tub-gal80*^{ts}, *w;Pdf-Red;MKRS/TM6*, and were donated by Justin Blau (New York University). The *cyc*^{01}, UAS-Δ-*cyc*, and UAS-Δ-*clk* stocks were donated by Paul Hardin (University of Texas).

Immunohistochemistry

<u>LN_vs PDF levels and neuronal morphology</u>: Brains of 6–8 day-old adult males or L3 larvae, depending on the experiment, were dissected between ZT2 and ZT3 in ice-cold Schneider's *Drosophila* Medium (S2) (Thermo Fisher, #21720024). They were fixed immediately after dissection in 2% Paraformaldehyde (PFA) in S2 for 30 minutes. Brains were then treated with blocking solution (5% goat serum in PBS-Tx 0.3%) for 1-hr at room temperature followed by incubation with primary antibodies at 4ºC for 24–48 hrs. The primary antibodies used were 1:3000 mouse anti-PDF (Developmental Hybridoma Bank) and 1:1000 rabbit anti-RFP (Rockland, #600-401-379-RTU). After incubation, the brains were rinsed 6 times in 0.3% PBS + Triton X-(PBT) after which they were incubated with Alexa-fluor conjugated secondary antibodies for 24-hr at 4ºC. The secondary antibodies used were 1:3000 Alexa-488 (Thermo Fisher, #A11029) and 1:1000 Alexa-568 (Thermo Fisher, #A11036). The brain samples were further washed 6 times with 0.3% PBT, cleaned and mounted on a clean, glass slide in Vectashield (Vector Laboratories, #H-1000-10) mounting media.

<u>PER Staining</u>: Brains of 6–8-day old males were dissected one hour before lights-on (ZT23) in ice-cold Schneider's *Drosophila* Medium (S2) (Thermo Fisher, #21720024). Immediately after dissection, they were fixed in 2% Paraformaldehyde (PFA) for 30 minutes and stained and mounted as described above. The primary antibodies used were 1:1000 rabbit anti-RFP (Rockland, #600-401-379-RTU) and 1:500 rat anti-PER (donated by Orie Shafer). The secondary antibodies

used were 1:1000 Alexa-568 (Thermo Fisher, #A11036) and 1:500 Alexa-488 (Thermo Fisher, #A21208).

Imaging, quantification, and Statistical Analysis

All images were acquired on an Olympus Fluoview 1000 laser-scanning confocal microscope using a 40x/1.10 NA FUMFL N objective (Olympus, Center Valley, PA) at the Advanced Science Research Center (ASRC-CUNY). For all experiments, only one hemisphere per brain was imaged (the right hemisphere, unless it was damaged, in which case we imaged the left hemisphere). The n represents the number of brains (flies) and N represents the number of independent experiments.

Quantification of adult LN_v morphology: We quantified the total projection length of the sLN_vs, the axonal projection length from the point of origin (POI) until the branching point, the degree of defasciculation of the sLN_v ventral projections (Fig S1A), and the dorsal termini branching (Fig S1C). If the axonal projection length went past the midline of the brain, the length was measured up to the midline. The projection length and partial projections length of the sLN_vs were quantified using Fiji [31] in ImageJ [32]. The length of the dorsal projection was determined by a line drawn from the point of intersection (POI) of the sLN_vs and the Optic Tract, until the end of the dorsal termini. The partial length of the dorsal projections was determined by a line drawn from the same point of intersection until the branching point (BP) of the sLN_vs at the dorsal termini. A modified Scholl Analysis [21] was used to measure the defasciculation of the sLN_v projections and the optic tract projection, which corresponds to the lLN_vs. (Fig S1A and 1C, respectively). Six concentric circles, each 25 microns (µm) apart, were placed around the same point of intersection used in the length measurements.

Quantification of larval sLN_v Morphology: We quantified total projection length of the sLN_vs, the axonal projection length until the branching point of the and the degree of branching in the sLN_v dorsal projections. The projection length, partial projections length, and area of the sLN_vs were quantified using the Fiji platform [31] in ImageJ [32]. The projection length was measured by a line drawn from a determined first point of intersection (POI) of each of the sLN_v cell bodies until the end of the dorsal termini. The partial length of the axonal projections was determined by a line drawn for the same point of intersection until the branching point (BP) of the sLN_vs at the dorsal

termini. A modified Scholl's Analysis was used to measure the branching of the sLN_v projections. Six concentric circles were places around the same branching point used in the length measurements. The concentric circles were each 12.5 µm away from each other so that the furthest circle was 75 µm away from the POI. The number of visible neurites of the sLN_vs that intersected with each circle, were counted and summed, giving the total number of intersecting neurons for the dorsal projections.

Quantification of PER levels: Single optical sections of either sLN_vs, lLN_vs or LN_ds were imaged using the same settings using a 40x/1.10 objective. PDF was used to identify the small and large LN_vs. The LN_ds were identified based on localization, size of the cell body, and morphology of the cluster. PER levels were determined through the normalization of nuclear staining within each cell to the background. An average value for each brain within a cluster was computed by averaging the values obtained from multiple cells within that cluster. Quantification was performed using images from 5-6 brains for each cluster at each timepoint.

Locomotor activity rhythm recording and analysis

DAM2 *Drosophila* Activity Monitors (TriKinetics, Waltham, MA) were used to record the locomotor activity rhythms of adult male flies, aged three- to five-days old, as previously described [61]. Flies were entrained to 12:12 LD cycles for at least five days, and then transferred to constant darkness (DD) for at least eight days, at a constant temperature of 28°C, unless otherwise specified. Free-running activity rhythms were analyzed with ClockLab software from Actimetrics (Wilmette, IL). We employed ClockLab's χ-square periodogram function, which was integrated into ClockLab software, for the analysis of rhythmicity, rhythmic power, and free-running period in individual flies, using a confidence level of 0.01 [33]. For each of the tested genotypes, only significant periodicities falling within the 14 to 34-hour range were taken into consideration. In instances where an individual fly exhibited multiple periodicities with peaks surpassing the significance threshold, only the period with the highest amplitude was utilized when calculating the average periods presented in Table 1. ClockLab assigns each peak in the χ-square periodogram both a "Power" value and a "Significance" value. The "Rhythmic Power" for each designated rhythmic fly was determined by subtracting the "Significance" value from the "Power" value associated with the predominant peak. Flies that did not exhibit a periodicity peak above the

significance threshold were categorized as "arrhythmic," and their period and rhythmic power were not included in the analysis.

Statistical Analysis

Pearson's D'Agostino normality tests were performed for all datasets. Depending on whether the data are normally distributed, statistical analyses were performed using either a one-way ANOVA with a Tukey's multiple comparisons test or a Kruskal-Wallis's test with a Dunn's multiple comparisons test for 3 and more groups, and a t-test for comparisons between 2 groups. Fisher's exact contingency tests were run to analyze the percent rhythmicity for the indicated genotypes under DD.

Materials and Reagents

REAGENT or RESOURCE	SOURCE	IDENTIFIER
Experimental Models: Organisms/Strains		
w;Pdf-dsRed,Pdf-Gal4;Tub-gal80^{ts}	J. Blau, NYU	
w;Pdf-dsRed;MKRS/TM6	J. Blau, NYU	
w;IF/CyO;uas-mef2	J. Blau, NYU	
w;;UAS-cyc^{RNAi42563}	Bloomington *Drosophila* Stock Center	BDSC 42563
w;;UAS-Clk$^{RNAi\ 42566}$	Bloomington *Drosophila* Stock Center	BDSC 42566
w^{1118};+;+	Bloomington *Drosophila* Stock Center	BDSC 3605
Canton-S	Bloomington *Drosophila* Stock Center	BDSC 64349
cyc^{01}	P. Hardin, University of Texas	BDSC 80929
;UAS-Δcyc;	P. Hardin, University of Texas	
;UAS-ΔClk	P. Hardin, University of Texas; Bloomington *Drosophila* Stock Center	BDSC 3618
Antibodies		

Rabbi anti-RFP (1:1000)	Rockland	#600-401-379-RTU
Mouse anti-PDF (1:3000)	Developmental Hybridoma Bank	
Rat anti-PER (1:500)	O. Shafer (ASRC CUNY)	
Anti-rabbit Alexa-568 (1:1000)	Thermo Fisher	A11036
Donkey anti-rat Alexa-488 (1:500)	Thermo Fisher	A21208
Anti-mouse Alexa-488 (1:3000)	Thermo Fisher	A11029
Software		
Fiji	http://fiji.sc	RRID: SCR_002285
Matlab R2018a	MathWorks, Natick	RRID: SCR_001622
GraphPad Prism 9.0	GraphPad Software	RRID: SCR_002798
DAM FileScan	Trikinetics	
ClockLab	Actimetrics	RRID:SCR_014309
Chemicals, Peptides, and Recombinant Proteins		
Vectashield Mounting Medium	Vector Laboratories	#H-1000-10
Premix PBS Buffer (10x)	Sigma-Aldrich	Cat# 11666789001
2% Paraformaldehyde (PFA)	Sigma-Aldrich	47608-250ML-F
Triton- X-100	Bio Basic	CAS#9002-93-1
Schneider's *Drosophila* Medium (S2)	Thermo Fisher	21720024
Other		
DAM2 *Drosophila* Activity Monitors	Trikinetics	
DAM Drosophila Environmental Monitors	Trikinetics	

Acknowledgments

We are very grateful to Justin Blau and Paul Hardin for their valuable feedback on various aspects of this project and for sharing fly lines with us. We are also grateful to Amanda González-Segarra, Aishwarya Ramakrishnan Iyer, and Orie Shafer for helpful comments on the manuscript, Annika Barber for helpful discussions, and Orie Shafer for the rat anti-PER antibody. The mouse anti-PDF antibody was obtained from the Developmental Studies Hybridoma Bank, created by the NICHD of the NIH and maintained at The University of Iowa, Department of Biology, Iowa City, IA 52242. Stocks obtained from the Bloomington *Drosophila* Stock Center (NIH P40OD018537) were used in this study. This work was supported by an NSF Grant (IOS-2239994) to M.P.F.

Figure Legends

Figure 1. *Cyc* downregulation in circadian pacemaker neurons prevents the formation of sLN$_v$s axon bundles. (A) Representative confocal images of anti-PDF staining in Canton-S control and *cyc^{01}* adult male brains. The sLN$_v$s and optic tract (OT) are indicated. Scale bar = 25 µm. The inserts on the right show the sLN$_v$ projections with the signal intensity adjusted for visibility in the *cyc^{01}* mutants. The top insert shows the distal (dorsal) and the bottom insert shows the proximal (ventral) area of the sLN$_v$ projections. Scale bar = 10 µm. (B) Representative confocal images of anti-RFP (magenta) staining in *Pdf-RFP* controls and *;Pdf-RFP;cyc^{01}* experimental flies. In the control brain the stereotypical branching point (BP) of the dorsal projections is indicated. Scale bar = 25 µm. Boxes in dashed lines indicate the proximal (1) and distal (2) projections, corresponding to the labeled projection images on the center and right panels. Scale bar =10 µm. (C-F) Quantification of the LN$_v$ morphology phenotypes from experimental flies in which a *cyc*^{RNAi} transgene is driven by a *Pdf*-Gal4;*Pdf-RFP* driver, compared to the heterozygote parental controls. The sLN$_v$ projection length until branching point (BP) (C), the total number of intersections of sLN$_v$ ventral projections (D), the total sLN$_v$ projection length (E), and the total number of intersections of the lLNv projections along the optic tract (OT) (F) are shown. Histograms show data from 3 independent experiments. Each dot corresponds to one brain. Flies were raised at 28˚C under LD conditions and dissected at ZT2-3. One-way ANOVAs followed by Tukey post-hoc test. Differences that are not significant are not indicated. * $P < 0.05$. *** $P < 0.001$. Error bars indicate SEM.

Figure 2. Constitutive *cyc* downregulation in *Pdf*+ cells leads to a reduction in PER levels and arrhythmicity under free-running conditions. (A,C,E) Representative confocal images of PER (green) and PDF (magenta) stainings in the sLN$_v$s (A), lLN$_v$s (C), and LN$_d$s (E) of *Pdf;tub-Gal80^{ts}>cyc^{RNAi}* experimental and *Pdf;tub-Gal80^{ts}*/+ control flies (n=5-6 brains per clock neuron group). Both lines also included a *Pdf-RFP* transgene. Scale bar= 10 µm. (B,D,F) T-Tests were used to compare nuclear PER intensity levels in the sLN$_v$s (B), lLN$_v$s (D), and LN$_d$s (F) in flies of the indicated genotypes. **P<0.01. Error bars indicate SEM. (G) Representative actograms of experimental (*Pdf;tub-Gal80^{ts} >cyc^{RNAi}*) and control (*Pdf;tub-Gal80^{ts}* /+ and *cyc^{RNAi}*/+) flies under 5 days of LD entrainment followed by 7 days of free running (DD). To allow comparison with

development-specific *cyc* downregulation, flies in this experiment were raised at 28˚C for their entire lifespan and the experiment was conducted at 28˚C. (H) Fisher's tests were employed to analyze the percent of rhythmic flies for the indicated genotypes under DD. Additional quantifications can be found in Table 1. R =% Rhythmic flies, AR= % Arrhythmic flies. *** P < 0.001.

Figure 3. Development-specific *cyc* downregulation in *Pdf*+ cells prevents the formation of sLN_v axonal bundles. (A) Representative confocal images of anti-PDF (green) and anti-RFP (magenta) stainings of brains of adult flies in which *cyc* was downregulated only during development. Each line also included a *Pdf-RFP* transgene. Flies were raised in LD at 28 ˚C, and transferred to 18 ˚C immediately after eclosion. Flies were kept at 18 ˚C for ~1 week and brains were dissected at ZT2-3. The sLN_vs, lLN_vs, OT, BP, and POI are labeled. Scale bar = 50 µm. The sLN_v projection length until branching point (BP) (B), the number of intersections of sLN_v ventral projections (C), the total sLN_v projection length (D), and the total number of intersections of the lLNv projections along the optic tract (OT) (E) are shown for flies in which *cyc* was downregulated in *Pdf*+ cells until eclosion. Two independent experiments were conducted. Kruskal-Wallis followed by Dunn's multiple comparisons tests ** P < 0.01. *** P < 0.001. *** P < 0.001. Error bars indicate SEM.

Figure 4. *Cyc* manipulations lead to aberrant sLN_v projections in larval clock neurons. (A-D) Developmental effects of *cyc* knockdown in the sLN_vs. (A) Representative confocal images of anti-RFP (magenta) labeling the sLN_vs of L3 larvae. The sLN_vs, POI, and BP are labeled. Scale bar =25 µm. (B-D) Kruskal-Wallis tests followed by Dunn's multiple comparisons tests were used to compare the projection length from the POI to the BP (B), the degree of sLN_v dorsal termini branching (C), and the total projection length (D). (E-H) Developmental effects of expressing a dominant-negative form of *cyc*, Δ-*cyc*, in the larval sLN_vs. (A) Representative confocal images of anti-RFP (magenta) staining in the sLN_vs of L3 larvae. 3 independent experiments were conducted for each genetic manipulation, each line also included a *Pdf-Red* transgene, and the larvae were kept in LD conditions 28˚C until dissection at ZT2-3. Kruskal-Wallis tests followed by Dunn's multiple comparisons tests compared the projection length from the POI to the BP (F), the degree

of sLN_v dorsal termini branching (G) and the total projection length (H). * P < 0.05. ** P < 0.01. *** P < 0.001. Error bars indicate SEM. Each dot corresponds to one brain.

Figure 5. *Clk* and *cyc* manipulations result in different morphology phenotypes in clock neurons. (A-E) Effects of constitutive *cyc* knockdown in the *Pdf*+ cells in adult brains. (A) Representative confocal images of anti-RFP (magenta) and anti-PDF (green) staining in the dorsal projections of the sLN_vs of the *Pdf;tub-Gal80ts >Clk*^{RNAi} experimental line. (B) Representative confocal images of anti-RFP (magenta) stainings in the sLN_vs adult fly brains of control (*Clk*^{RNAi} /+ and *Pdf;tub-Gal80*^{ts}/+), and experimental (*Pdf;tub-Gal80ts >Clk*^{RNAi}) lines are shown. Each line also included a *Pdf-Red* transgene. Scale bar = 25 µm. (C-E) Quantification of sLN_v morphology using Kruskal-Wallis tests followed by Dunn's multiple comparisons tests of the length until branching point (C), the total number of axonal crosses of the sLN_vs (D), and the total number of axonal crosses after the BP (E). (F-I) Effects of constitutive Δ-*Clk* expression in the *Pdf*+ cells in adult brains. (F) Representative confocal images of the UAS-Δ-*Clk* control and the *Pdf;tub-Gal80ts*> Δ-*Clk* experimental line. (G-I) Kruskal-Wallis tests followed by Dunn's multiple comparisons tests compared the length until branching point (F), the number of axonal crosses in the sLN_v projections (G), and the total sLN_v projection length (H). Each dot corresponds to one brain. For each genotype, flies were raised under LD at 28˚C and experiments were conducted at 28˚C at ZT2-3. * P < 0.05. *** P < 0.001. Error bars indicate SEM.

Figure 6. Expressing Δ-*Clk* in the sLN_vs leads to axonal morphology phenotypes in larvae. (A) Representative confocal images of anti-RFP (magenta) staining in the sLN_vs when Δ-*Clk* was expressed in *Pdf*+ neurons in L3 larvae. Each line also included a *Pdf-Red* transgene. Scale bar = 25 µm. For each genotype, flies were raised under LD conditions at 28˚C and dissected at ZT2-3. Kruskal Wallis tests followed by Dunn's multiple comparisons tests were used to compare the length until the BP (B), the degree of sLN_v dorsal termini branching (C), and the total projection length (D). * P < 0.05. ** P < 0.01. *** P < 0.001. Error bars indicate SEM. Each dot corresponds to one brain.

Supplemental Figures

Supplementary Figure 1. Quantification of defasciculation (ventral projections) and branching (dorsal projections) in the LNvs. (A-C) Representative confocal images of anti-RFP (magenta) stainings in adult (A,C), and L3 larval (B) control brains. The sLN_vs, OT, POI, and BP are indicated. Scale bars indicates 50 µm (A,C) and 25 µm (B). (A) To determine degree of defasciculation of the sLN_v ventral projections in adult brains, 6 concentric circles separated by is 25 µm were centered at the point of intersection (POI), where the projections of the sLN_vs and those of the lLN_vs intersect. This is often where the sLN_v cell bodies are located, but their position is variable. The most distant circle does not reach the main branching point (BP) in control brains, therefore the dorsal termini, where PDF rhythmically accumulates, are not included. The number of intersections between either the sLNvs or the lLN_vs with each concentric circle where quantified. (B) Dorsal projection branching in the larval sLN_vs was measured counting the number of intersections the sLN_vs had at each of 6 concentric circles separated by 12.5 µm. (C) Adult sLN_v dorsal projection branching was measured counting the number of intersections the sLNvs had at each of 8 concentric circles separated by 12.5 µm. This was adapted from a previous study [36] to adequately capture the hyper expended phenotype of in *Pdf;tub-Gal80^{ts}*> Δ-*Clk* experimental brains.

Supplementary Figure 2. Δ-*cyc* expression in *Pdf*+ cells prevent the formation of the sLN_vs axonal bundles. (A) Representative brain confocal images of anti-PDF (green) and anti-RFP (magenta) staining in the sLN_vs of flies in which Δ-*cyc* was constitutively expressed in the *Pdf*+ cells using a *Pdf;tub-Gal80^{ts}* driver. The images are representative of 2 independent experiments. Scale bar = 50 µm. Flies were raised under LD at 28˚C and kept at 28˚C for ~1 week after eclosion before brain dissections at ZT2-3. Kruskal-Wallis tests followed by Dunn's multiple comparisons tests were used to compare the sLN_v projection length until branching point (B), the total number of intersections of the sLN_v ventral projections (C), the full sLN_v projection length (D), and the total lLN_v intersections (E). * $P < 0.05$. ** $P < 0.01$. *** $P < 0.001$. Error bars indicate SEM.

Supplementary Figure 3. Adult-specific *cyc* knockdown has no effect on axonal morphology and development-specific *cyc* knockdown leads to arrhythmicity. (A) Representative confocal images of anti-PDF and anti-RFP (magenta) staining in the sLN_vs when *cyc* was downregulated exclusively after eclosion. The images are representative of 2 independent experiments. Scale bar

= 50 µm. Each line also included a *Pdf-Red* transgene. Flies were raised under LD at 18˚C, and transferred to 28˚C immediately after eclosion. Kruskal-Wallis tests followed by Dunn's multiple comparisons tests were used to quantify projection length until BP (B), the total number of intersections of the sLN_v ventral projections (C), the full sLN_v projection length (D), and the total lLN_v intersections (E). (F-H). Behavioral consequences of development- specific *cyc* knockdown. Flies were raised in LD at 28 ˚C, before being transferred to 18 ˚C upon eclosion. Experiments were conducted at 18 ˚C (F) Representative actograms of flies of the indicated genotypes under free-running (See table 1 for n and additional quantifications). (G-H) Percent rhythmicity for the indicated genotypes under DD. Rhythmic is labeled as R and arrhythmic is labeled as AR. Fisher's exact contingency tests were run to analyze the percent rhythmicity for the indicated genotypes under DD. * $P < 0.05$. *** $P < 0.001$. Error bars indicate SEM.

Supplementary Figure 4. Expressing Clk^{RNAi} in the LN_vs results in rhythmicity loss under free-running conditions. (A) Representative actograms of flies of the indicated genotypes under free running conditions. The flies were raised in LD at 28˚C and experiments were conducted at 28˚C. (B) Fisher's tests were employed to compare the percent of rhythmic flies of each genotype (additional quantifications can be found in Table 1). R= % rhythmic flies, AR= % arrhythmic flies. (C-D) Effects of Clk^{RNAi} expression in the *Pdf*+ cells in adult brains. Neither the sLNv total projection length (C) nor the lLNv projections (D) were affected. (E) Expression of Δ-*Clk* in the *Pdf*+ cells in adult brains does not affect the lLNv projections. Kruskal-Wallis tests followed by Dunn's multiple comparisons tests. Each dot corresponds to one brain. Flies were raised under LD at 28˚C and experiments were conducted at 28˚C at ZT2-3. Error bars indicate SEM.

Supplementary Figure 5. *Clk* knockdown in the larval sLN_vs has no morphological phenotypes. (A) Representative confocal images of anti-RFP (magenta) staining in the sLN_vs when Clk^{RNAi} was expressed in L3 larvae. The sLN_vs, POI, and BP are labeled. The UAS, Gal4, and experimental lines are indicated. Each line also contains a *Pdf-Red* transgene. Scale bar = 25 µm. Kruskal-Wallis tests followed by Dunn's multiple comparisons tests compared the projection length from the POI to the BP in microns (B), the total number of axonal intersections with the polar circle (C), and the total projection length from the POI in microns (D). Significant differences

between the morphological parameters measured are marked and differences that are not significant are not marked. * $P < 0.05$. Error bars indicate SEM.

References

1. Herzog, E.D. (2007). Neurons and networks in daily rhythms. Nat Rev Neurosci *8*, 790-802.
2. Taghert, P.H., and Nitabach, M.N. (2012). Peptide neuromodulation in invertebrate model systems. Neuron *76*, 82-97.
3. Sehgal, A., Price, J., and Young, M.W. (1992). Ontogeny of a biological clock in Drosophila melanogaster. Proc Natl Acad Sci U S A *89*, 1423-1427.
4. Helfrich-Forster, C. (2003). The neuroarchitecture of the circadian clock in the brain of Drosophila melanogaster. Microsc Res Tech *62*, 94-102.
5. Shafer, O.T., Helfrich-Forster, C., Renn, S.C., and Taghert, P.H. (2006). Reevaluation of Drosophila melanogaster's neuronal circadian pacemakers reveals new neuronal classes. J Comp Neurol *498*, 180-193.
6. Schubert, F.K., Hagedorn, N., Yoshii, T., Helfrich-Forster, C., and Rieger, D. (2018). Neuroanatomical details of the lateral neurons of Drosophila melanogaster support their functional role in the circadian system. J Comp Neurol *526*, 1209-1231.
7. Hardin, P.E., Hall, J.C., and Rosbash, M. (1990). Feedback of the Drosophila period gene product on circadian cycling of its messenger RNA levels. Nature *343*, 536-540.
8. Dubowy, C., and Sehgal, A. (2017). Circadian Rhythms and Sleep in Drosophila melanogaster. Genetics *205*, 1373-1397.
9. Cyran, S.A., Buchsbaum, A.M., Reddy, K.L., Lin, M.C., Glossop, N.R., Hardin, P.E., Young, M.W., Storti, R.V., and Blau, J. (2003). vrille, Pdp1, and dClock form a second feedback loop in the Drosophila circadian clock. Cell *112*, 329-341.
10. Glossop, N.R.J., Houl, J.H., Zheng, H., Ng, F.S., Dudek, S.M., and Hardin, P.E. (2003). VRILLE Feeds Back to Control Circadian Transcription of Clock in the Drosophila Circadian Oscillator. Neuron *37*, 249-261.
11. Liu, T., Mahesh, G., Houl, J.H., and Hardin, P.E. (2015). Circadian Activators Are Expressed Days before They Initiate Clock Function in Late Pacemaker Neurons from Drosophila. The Journal of Neuroscience *35*, 8662-8671.
12. Rutila, J.E., Suri, V., Le, M., So, W.V., Rosbash, M., and Hall, J.C. (1998). CYCLE is a second bHLH-PAS clock protein essential for circadian rhythmicity and transcription of Drosophila period and timeless. Cell *93*, 805-814.
13. Dong, Z., Zhang, G., Qu, M., Gimple, R.C., Wu, Q., Qiu, Z., Prager, B.C., Wang, X., Kim, L.J.Y., Morton, A.R., et al. (2019). Targeting Glioblastoma Stem Cells through Disruption of the Circadian Clock. Cancer Discov *9*, 1556-1573.
14. Wagner, P.M., Prucca, C.G., Velazquez, F.N., Sosa Alderete, L.G., Caputto, B.L., and Guido, M.E. (2021). Temporal regulation of tumor growth in nocturnal mammals: In vivo studies and chemotherapeutical potential. FASEB J *35*, e21231.
15. Kondratova, A.A., Dubrovsky, Y.V., Antoch, M.P., and Kondratov, R.V. (2010). Circadian clock proteins control adaptation to novel environment and memory formation. Aging (Albany NY) *2*, 285-297.
16. Kondratov, R.V., Kondratova, A.A., Gorbacheva, V.Y., Vykhovanets, O.V., and Antoch, M.P. (2006). Early aging and age-related pathologies in mice deficient in BMAL1, the core componentof the circadian clock. Genes Dev *20*, 1868-1873.

17. Zheng, Y., Pan, L., Wang, F., Yan, J., Wang, T., Xia, Y., Yao, L., Deng, K., Zheng, Y., Xia, X., et al. (2023). Neural function of Bmal1: an overview. Cell & Bioscience *13*, 1.
18. Peschel, N., and Helfrich-Förster, C. (2011). Setting the clock – by nature: Circadian rhythm in the fruitfly Drosophila melanogaster. FEBS Letters *585*, 1435-1442.
19. Ma, D., Przybylski, D., Abruzzi, K.C., Schlichting, M., Li, Q., Long, X., and Rosbash, M. (2021). A transcriptomic taxonomy of Drosophila circadian neurons around the clock. eLife *10*, e63056.
20. Shafer, O.T., Gutierrez, G.J., Li, K., Mildenhall, A., Spira, D., Marty, J., Lazar, A.A., and Fernandez, M.P. (2022). Connectomic analysis of the Drosophila lateral neuron clock cells reveals the synaptic basis of functional pacemaker classes. Elife *11*.
21. Helfrich-Forster, C. (2005). Neurobiology of the fruit fly's circadian clock. Genes Brain Behav *4*, 65-76.
22. Abruzzi, K.C., Zadina, A., Luo, W., Wiyanto, E., Rahman, R., Guo, F., Shafer, O., and Rosbash, M. (2017). RNA-seq analysis of Drosophila clock and non-clock neurons reveals neuron-specific cycling and novel candidate neuropeptides. PLoS Genet *13*, e1006613.
23. Rieger, D., Shafer, O.T., Tomioka, K., and Helfrich-Forster, C. (2006). Functional analysis of circadian pacemaker neurons in Drosophila melanogaster. J Neurosci *26*, 2531-2543.
24. Murad, A., Emery-Le, M., and Emery, P. (2007). A subset of dorsal neurons modulates circadian behavior and light responses in Drosophila. Neuron *53*, 689-701.
25. Grima, B., Chelot, E., Xia, R., and Rouyer, F. (2004). Morning and evening peaks of activity rely on different clock neurons of the Drosophila brain. Nature *431*, 869-873.
26. Stoleru, D., Peng, Y., Agosto, J., and Rosbash, M. (2004). Coupled oscillators control morning and evening locomotor behaviour of Drosophila. Nature *431*, 862-868.
27. Ewer, J., Frisch, B., Hamblen-Coyle, M.J., Rosbash, M., and Hall, J.C. (1992). Expression of the period clock gene within different cell types in the brain of Drosophila adults and mosaic analysis of these cells' influence on circadian behavioral rhythms. J Neurosci *12*, 3321-3349.
28. Frisch, B., Hardin, P.E., Hamblen-Coyle, M.J., Rosbash, M., and Hall, J.C. (1994). A promoterless period gene mediates behavioral rhythmicity and cyclical per expression in a restricted subset of the Drosophila nervous system. Neuron *12*, 555-570.
29. Renn, S.C., Park, J.H., Rosbash, M., Hall, J.C., and Taghert, P.H. (1999). A pdf neuropeptide gene mutation and ablation of PDF neurons each cause severe abnormalities of behavioral circadian rhythms in Drosophila. Cell *99*, 791-802.
30. Shafer, O.T., and Yao, Z. (2014). Pigment-Dispersing Factor Signaling and Circadian Rhythms in Insect Locomotor Activity. Curr Opin Insect Sci *1*, 73-80.
31. Park, J.H., Helfrich-Forster, C., Lee, G., Liu, L., Rosbash, M., and Hall, J.C. (2000). Differential regulation of circadian pacemaker output by separate clock genes in Drosophila. Proc Natl Acad Sci U S A *97*, 3608-3613.
32. Klose, M.K., Bruchez, M.P., Deitcher, D.L., and Levitan, E.S. (2021). Temporally and spatially partitioned neuropeptide release from individual clock neurons. Proc Natl Acad Sci U S A *118*.
33. Shang, Y., Griffith, L.C., and Rosbash, M. (2008). Light-arousal and circadian photoreception circuits intersect at the large PDF cells of the Drosophila brain. Proc Natl Acad Sci U S A *105*, 19587-19594.

34. Helfrich-Forster, C., Shafer, O.T., Wulbeck, C., Grieshaber, E., Rieger, D., and Taghert, P. (2007). Development and morphology of the clock-gene-expressing lateral neurons of Drosophila melanogaster. J Comp Neurol *500*, 47-70.
35. Helfrich-Forster, C., and Homberg, U. (1993). Pigment-dispersing hormone-immunoreactive neurons in the nervous system of wild-type Drosophila melanogaster and of several mutants with altered circadian rhythmicity. J Comp Neurol *337*, 177-190.
36. Fernandez, M.P., Berni, J., and Ceriani, M.F. (2008). Circadian remodeling of neuronal circuits involved in rhythmic behavior. PLoS Biol *6*, e69.
37. Petsakou, A., Sapsis, Themistoklis P., and Blau, J. (2015). Circadian Rhythms in Rho1 Activity Regulate Neuronal Plasticity and Network Hierarchy. Cell *162*, 823-835.
38. Gorostiza, E.A., Depetris-Chauvin, A., Frenkel, L., Pírez, N., and Ceriani, María F. (2014). Circadian Pacemaker Neurons Change Synaptic Contacts across the Day. Current Biology *24*, 2161-2167.
39. Herrero, A., Duhart, J.M., and Ceriani, M.F. (2017). Neuronal and Glial Clocks Underlying Structural Remodeling of Pacemaker Neurons in Drosophila. Frontiers in Physiology *8*.
40. Depetris-Chauvin, A., Fernández-Gamba, Á., Gorostiza, E.A., Herrero, A., Castaño, E.M., and Ceriani, M.F. (2014). Mmp1 Processing of the PDF Neuropeptide Regulates Circadian Structural Plasticity of Pacemaker Neurons. PLOS Genetics *10*, e1004700.
41. Blau, J., and Young, M.W. (1999). Cycling vrille Expression Is Required for a Functional Drosophila Clock. Cell *99*, 661-671.
42. Tanoue, S., Krishnan, P., Krishnan, B., Dryer, S.E., and Hardin, P.E. (2004). Circadian clocks in antennal neurons are necessary and sufficient for olfaction rhythms in Drosophila. Curr Biol *14*, 638-649.
43. Gunawardhana, K.L., and Hardin, P.E. (2017). VRILLE Controls PDF Neuropeptide Accumulation and Arborization Rhythms in Small Ventrolateral Neurons to Drive Rhythmic Behavior in Drosophila. Curr Biol *27*, 3442-3453 e3444.
44. Goda, T., Mirowska, K., Currie, J., Kim, M.H., Rao, N.V., Bonilla, G., and Wijnen, H. (2011). Adult circadian behavior in Drosophila requires developmental expression of cycle, but not period. PLoS Genet *7*, e1002167.
45. Ruben, M., Drapeau, M.D., Mizrak, D., and Blau, J. (2012). A mechanism for circadian control of pacemaker neuron excitability. J Biol Rhythms *27*, 353-364.
46. Sholl, D.A. (1953). Dendritic organization in the neurons of the visual and motor cortices of the cat. J Anat *87*, 387-406.
47. Collins, B., Kane, Elizabeth A., Reeves, David C., Akabas, Myles H., and Blau, J. (2012). Balance of Activity between LNvs and Glutamatergic Dorsal Clock Neurons Promotes Robust Circadian Rhythms in Drosophila. Neuron *74*, 706-718.
48. Lorber, C., Leleux, S., Stanewsky, R., and Lamaze, A. (2022). Light triggers a network switch between circadian morning and evening oscillators controlling behaviour during daily temperature cycles. PLOS Genetics *18*, e1010487.
49. Siwicki, K.K., Eastman, C., Petersen, G., Rosbash, M., and Hall, J.C. (1988). Antibodies to the period gene product of Drosophila reveal diverse tissue distribution and rhythmic changes in the visual system. Neuron *1*, 141-150.

50. Hendricks, J.C., Lu, S., Kume, K., Yin, J.C., Yang, Z., and Sehgal, A. (2003). Gender dimorphism in the role of cycle (BMAL1) in rest, rest regulation, and longevity in Drosophila melanogaster. J Biol Rhythms *18*, 12-25.
51. Helfrich-Forster, C. (1997). Development of pigment-dispersing hormone-immunoreactive neurons in the nervous system of Drosophila melanogaster. J Comp Neurol *380*, 335-354.
52. McGuire, S.E., Mao, Z., and Davis, R.L. (2004). Spatiotemporal gene expression targeting with the TARGET and gene-switch systems in Drosophila. Sci STKE *2004*, pl6.
53. Keene, A.C., Duboue, E.R., McDonald, D.M., Dus, M., Suh, G.S., Waddell, S., and Blau, J. (2010). Clock and cycle limit starvation-induced sleep loss in Drosophila. Curr Biol *20*, 1209-1215.
54. Sivachenko, A., Li, Y., Abruzzi, K.C., and Rosbash, M. (2013). The transcription factor Mef2 links the Drosophila core clock to Fas2, neuronal morphology, and circadian behavior. Neuron *79*, 281-292.
55. Houl, J.H., Ng, F., Taylor, P., and Hardin, P.E. (2008). CLOCK expression identifies developing circadian oscillator neurons in the brains of Drosophila embryos. BMC Neurosci *9*, 119.
56. Herrero, A., Yoshii, T., Ispizua, J.I., Colque, C., Veenstra, J.A., Muraro, N.I., and Ceriani, M.F. (2020). Coupling Neuropeptide Levels to Structural Plasticity in Drosophila Clock Neurons. Curr Biol *30*, 3154-3166 e3154.
57. Gorostiza, E.A., and Ceriani, M.F. (2013). Retrograde Bone Morphogenetic Protein Signaling Shapes a Key Circadian Pacemaker Circuit. The Journal of Neuroscience *33*, 687-696.
58. Nagoshi, E., Sugino, K., Kula, E., Okazaki, E., Tachibana, T., Nelson, S., and Rosbash, M. (2010). Dissecting differential gene expression within the circadian neuronal circuit of Drosophila. Nat Neurosci *13*, 60-68.
59. Zhao, J., Kilman, V.L., Keegan, K.P., Peng, Y., Emery, P., Rosbash, M., and Allada, R. (2003). Drosophila clock can generate ectopic circadian clocks. Cell *113*, 755-766.
60. Liu, T., Mahesh, G., Yu, W., and Hardin, P.E. (2017). CLOCK stabilizes CYCLE to initiate clock function in Drosophila. Proc Natl Acad Sci U S A *114*, 10972-10977.
61. Fernandez, M.P., Pettibone, H.L., Bogart, J.T., Roell, C.J., Davey, C.E., Pranevicius, A., Huynh, K.V., Lennox, S.M., Kostadinov, B.S., and Shafer, O.T. (2020). Sites of Circadian Clock Neuron Plasticity Mediate Sensory Integration and Entrainment. Curr Biol *30*, 2225-2237 e2225.

Figure 1

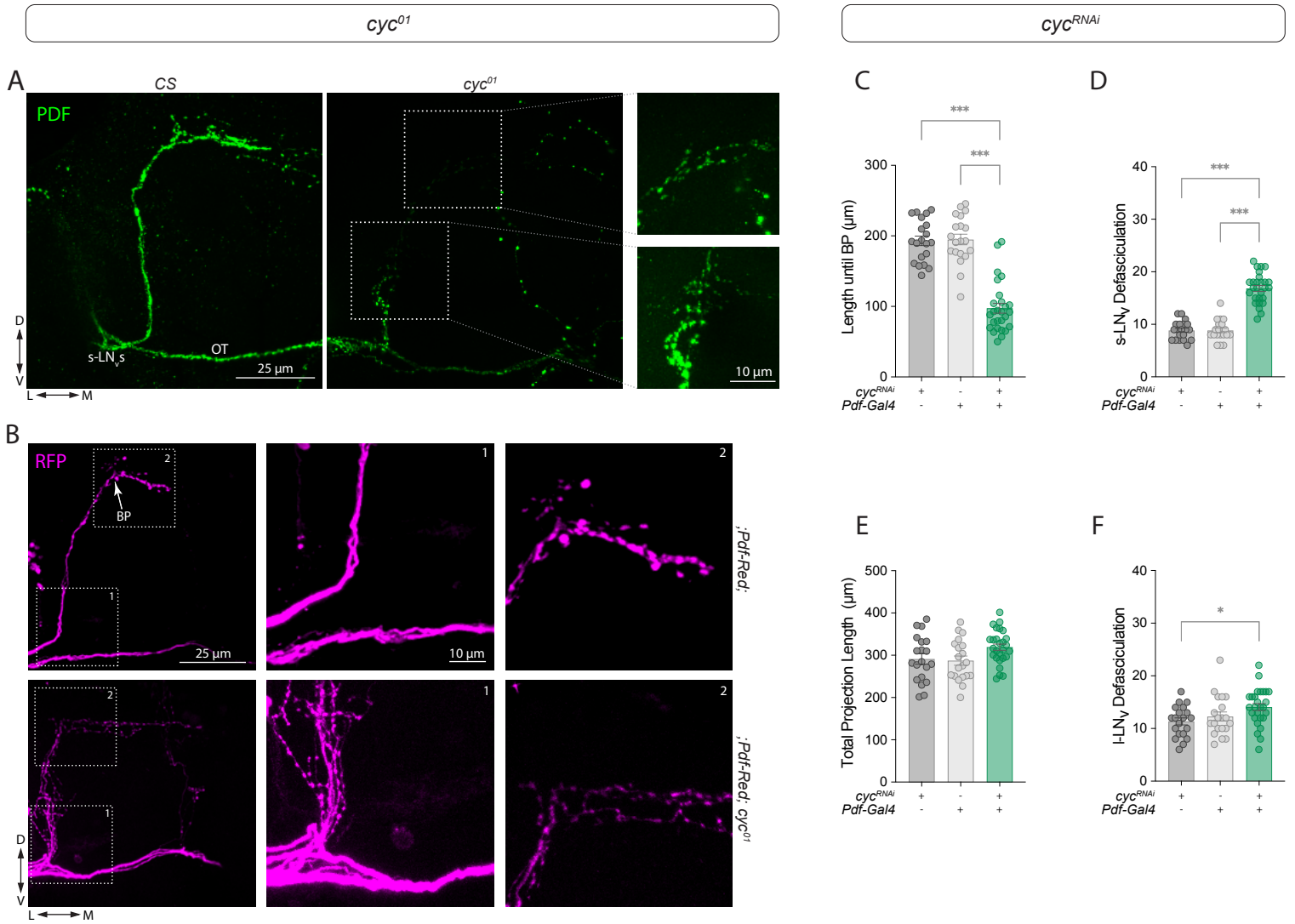
cyc01
cycRNAi
A
CS
cyc01
PDF
s-LNvs
OT
25 µm
10 µm
D
V
L
M
B
RFP
BP
1
2
25 µm
10 µm
;Pdf-Red;
;Pdf-Red; cyc01
C
D
E
F
Length until BP (µm)
s-LNv Defasciculation
Total Projection Length (µm)
l-LNv Defasciculation
***
*
cycRNAi
Pdf-Gal4

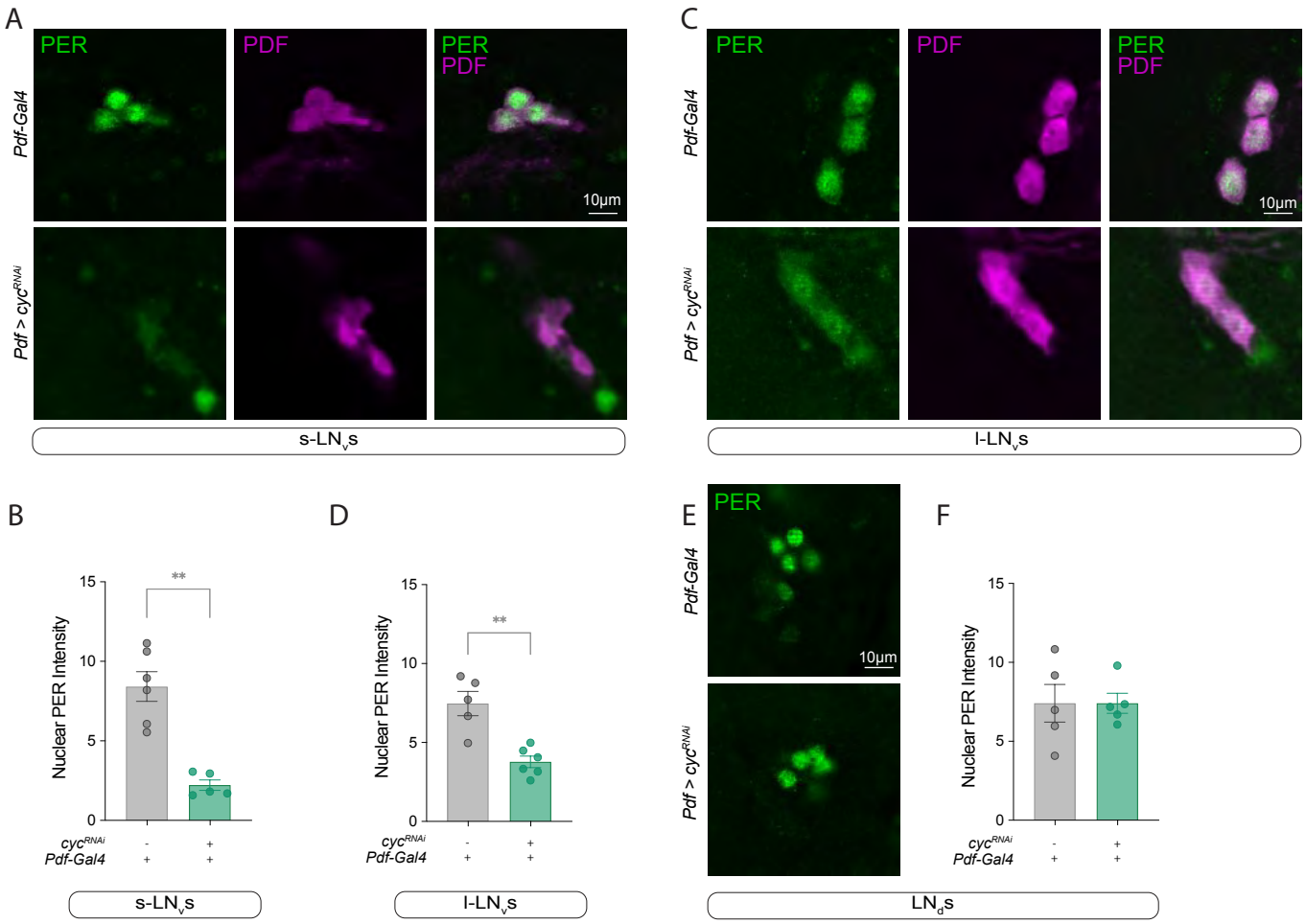
A
PER
PDF
PER
PDF
10μm
Pdf-Gal4
Pdf > cycRNAi
s-LNvs
C
PER
PDF
PER
PDF
10μm
Pdf-Gal4
Pdf > cycRNAi
l-LNvs
B
Nuclear PER Intensity
15
10
5
0
**
cycRNAi - +
Pdf-Gal4 + +
s-LNvs
D
Nuclear PER Intensity
15
10
5
0
**
cycRNAi - +
Pdf-Gal4 + +
l-LNvs
E
PER
10μm
Pdf-Gal4
Pdf > cycRNAi
F
Nuclear PER Intensity
15
10
5
0
cycRNAi - +
Pdf-Gal4 + +
LNds

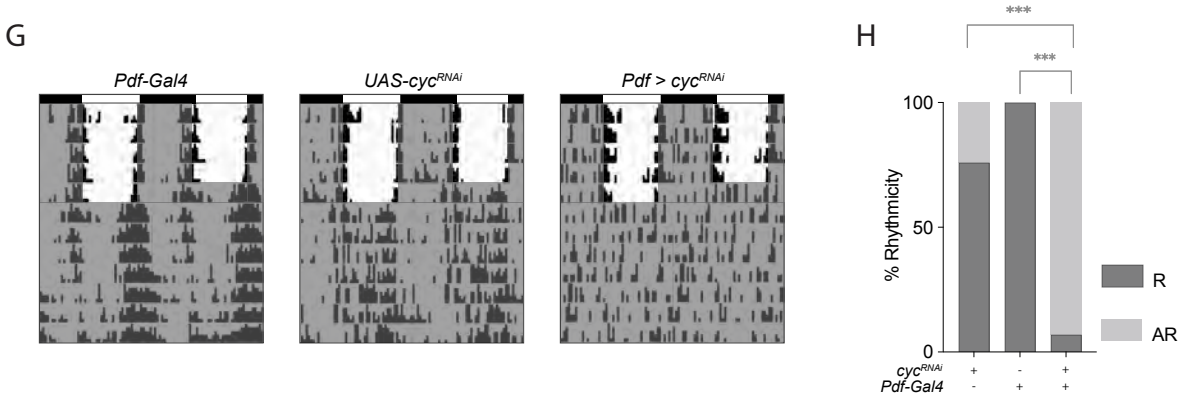
G
Pdf-Gal4
UAS-cycRNAi
Pdf > cycRNAi
H
***
***
% Rhythmicity
100
50
0
R
AR
cycRNAi + - +
Pdf-Gal4 - + +

Development-specific *cyc* silencing

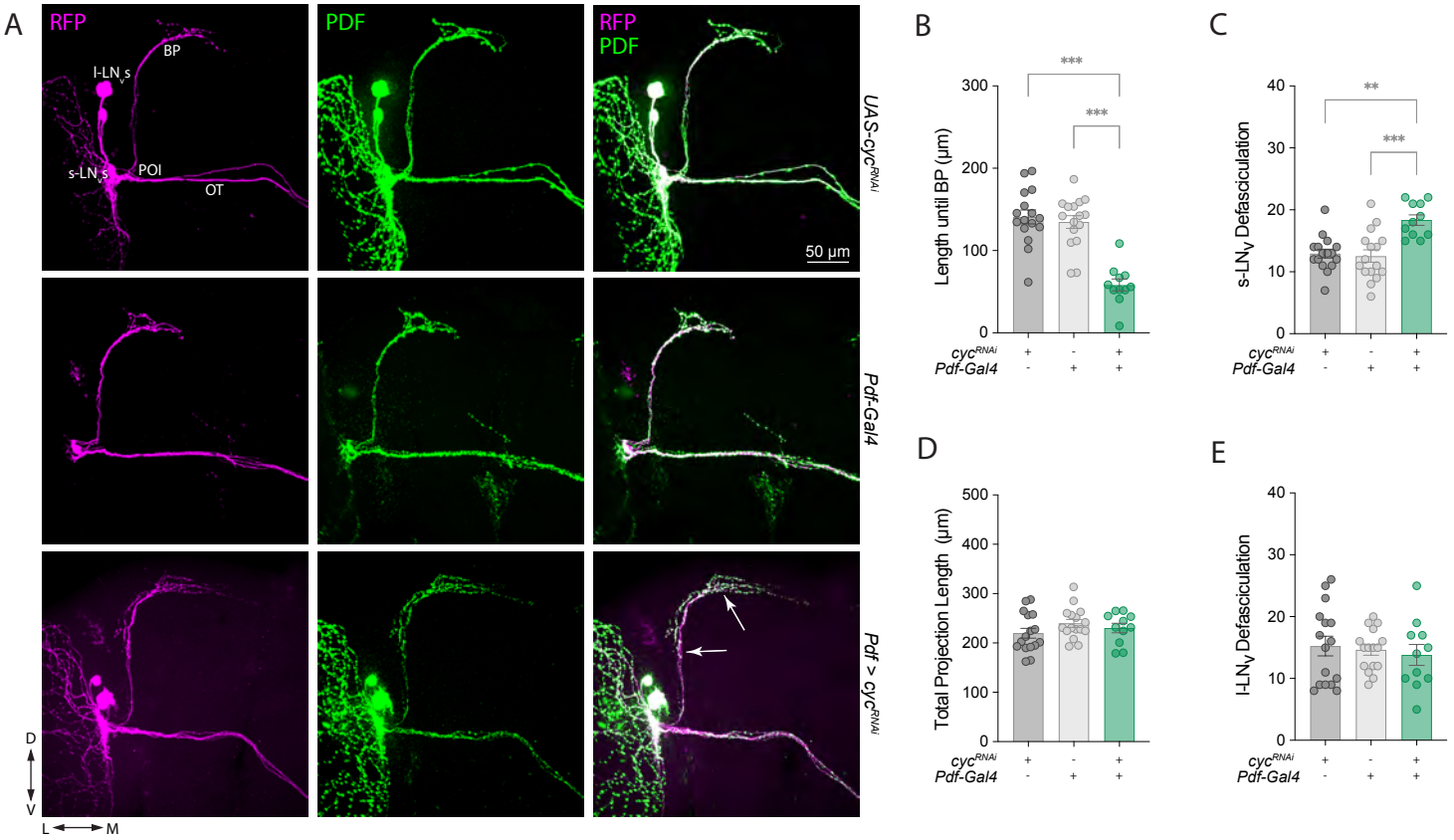

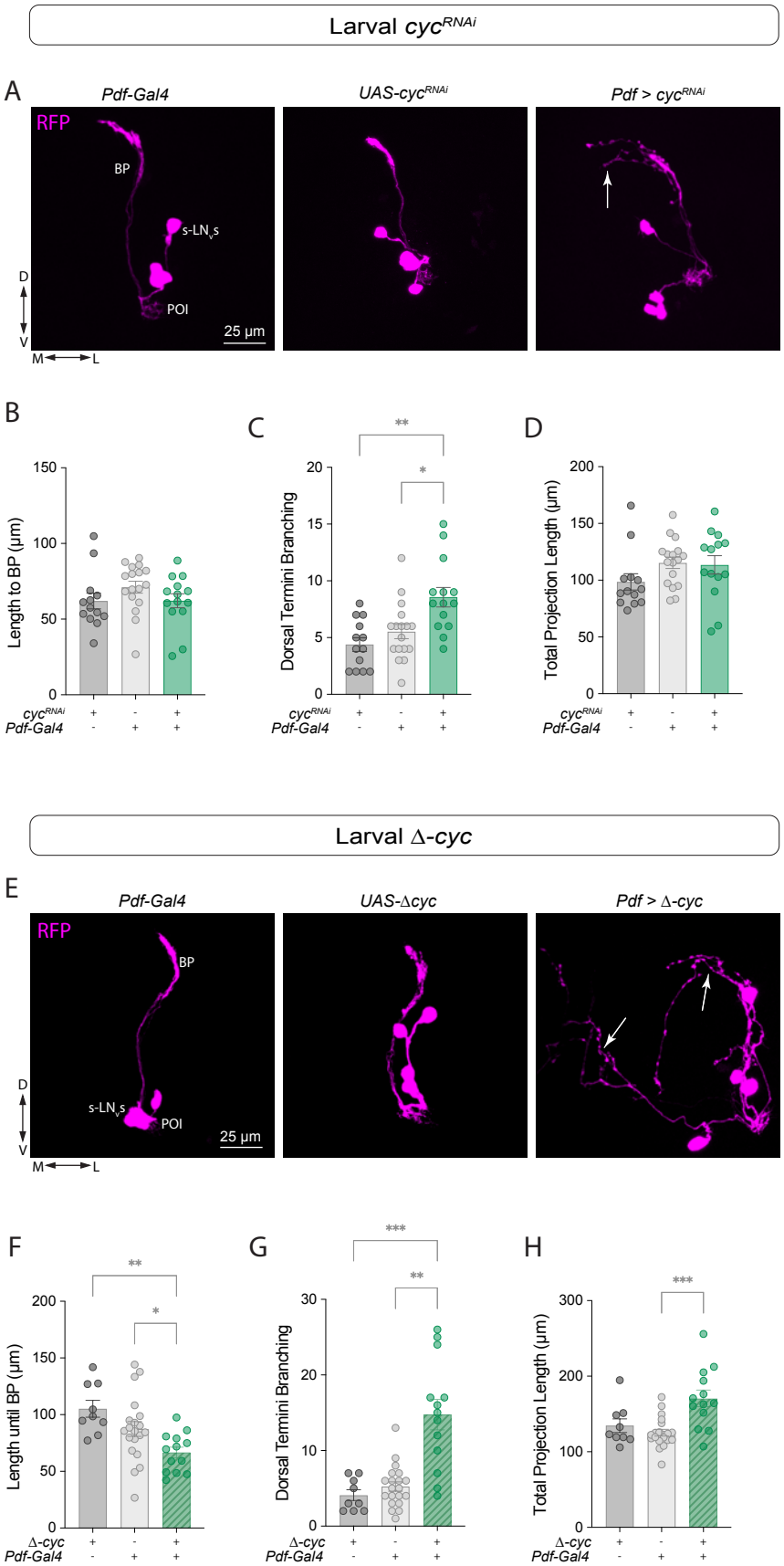
Larval cycRNAi
A
Pdf-Gal4
UAS-cycRNAi
Pdf > cycRNAi
RFP
BP
s-LNvs
POI
25 µm
D
V
M
L
B
Length to BP (µm)
C
Dorsal Termini Branching
D
Total Projection Length (µm)
cycRNAi
Pdf-Gal4
Larval Δ-cyc
E
Pdf-Gal4
UAS-Δcyc
Pdf > Δ-cyc
RFP
BP
s-LNvs
POI
25 µm
F
Length until BP (µm)
G
Dorsal Termini Branching
H
Total Projection Length (µm)
Δ-cyc
Pdf-Gal4

Adult *Clk*^{RNAi}

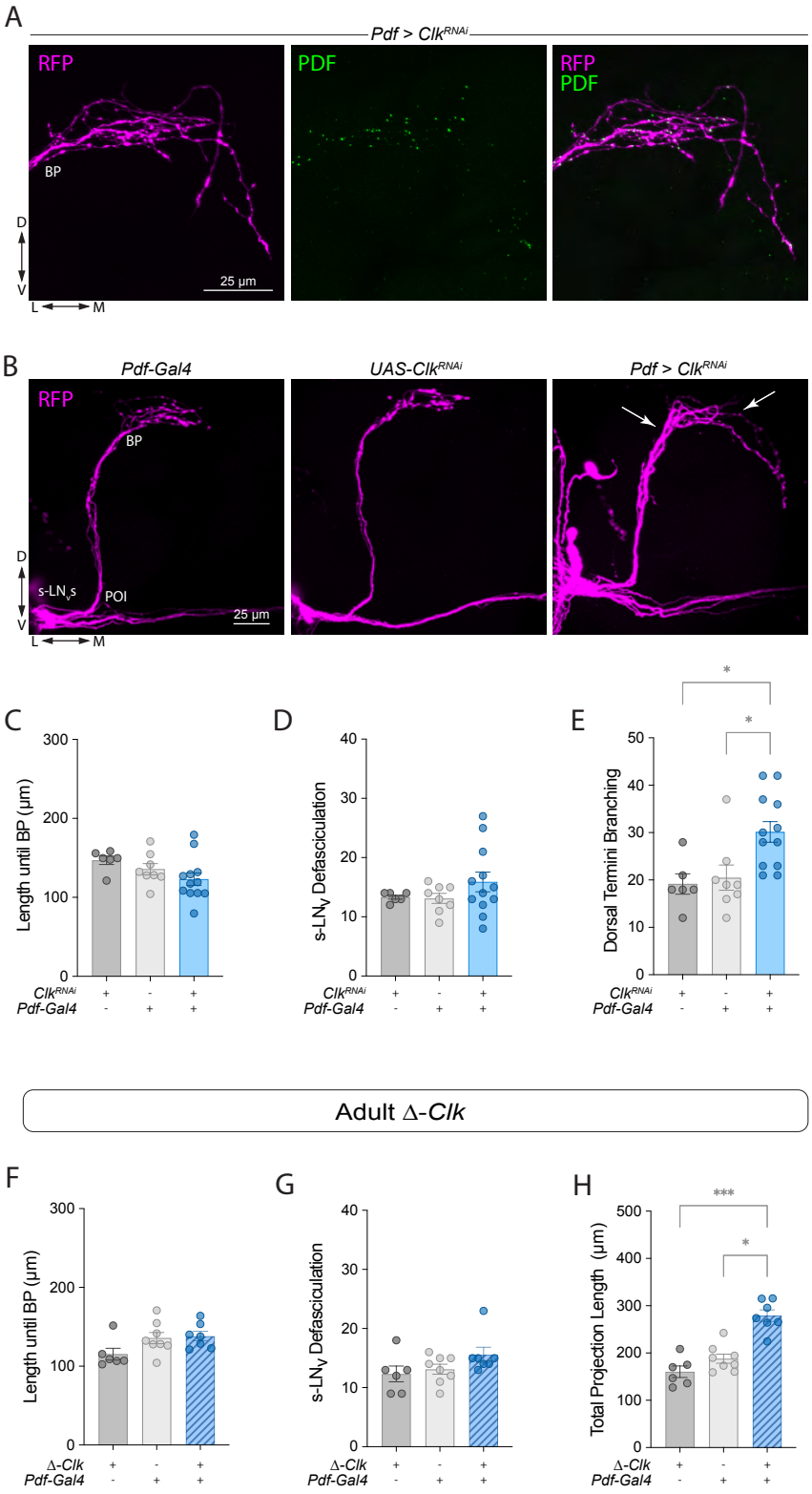

Larval Δ-*Clk*

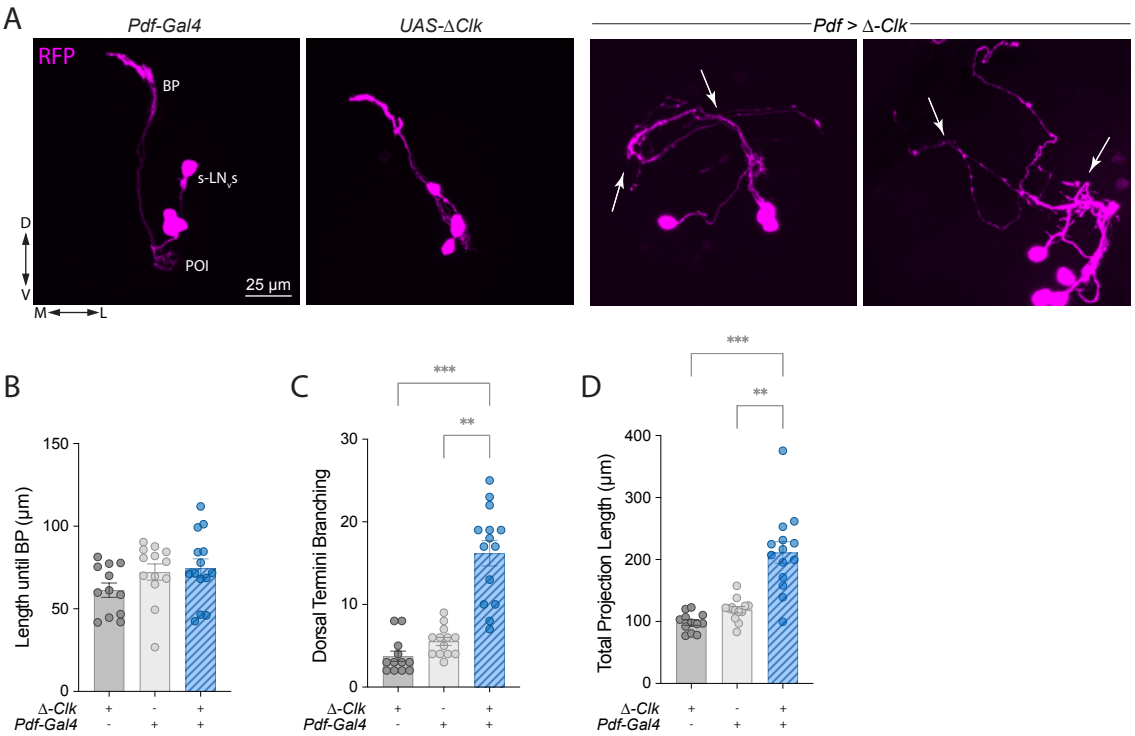
A
Pdf-Gal4
UAS-ΔClk
Pdf > Δ-Clk
RFP
BP
s-LNvs
POI
25 µm
D
V
M
L
B
Length until BP (µm)
150
100
50
0
Δ-Clk + - +
Pdf-Gal4 - + +
C
Dorsal Termini Branching
30
20
10
0
***
**
Δ-Clk + - +
Pdf-Gal4 - + +
D
Total Projection Length (µm)
400
300
200
100
0
***
**
Δ-Clk + - +
Pdf-Gal4 - + +

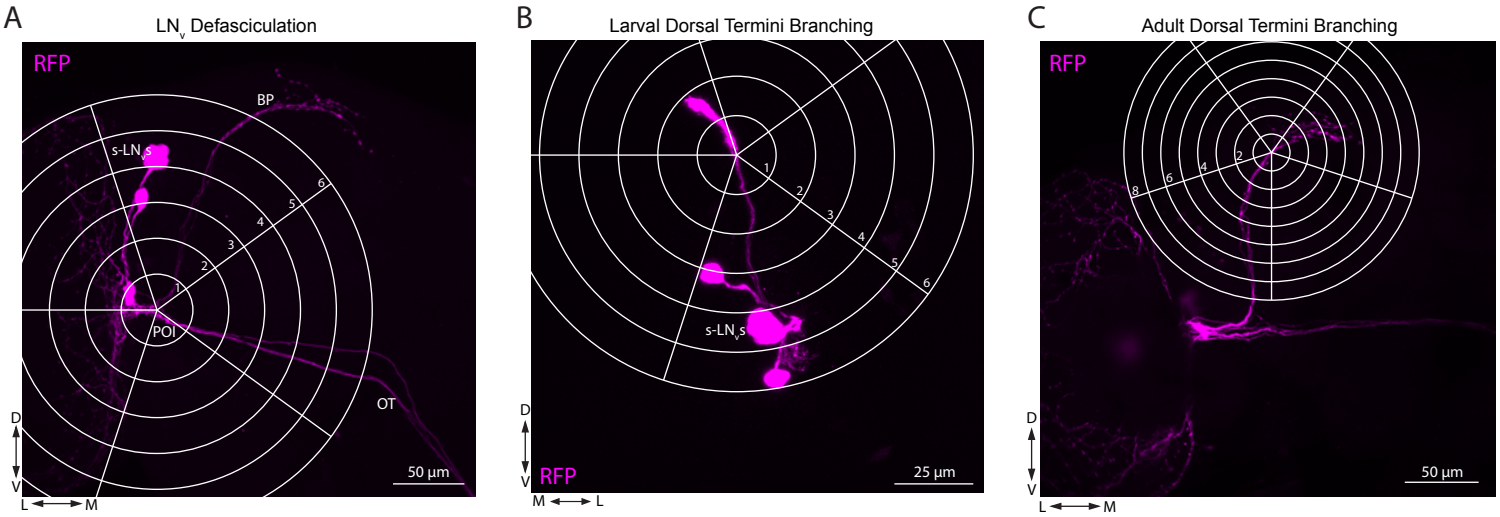
A
LNv Defasciculation
RFP
BP
s-LNvs
POI
OT
1
2
3
4
5
6
50 µm
D
V
L
M
B
Larval Dorsal Termini Branching
s-LNvs
RFP
25 µm
C
Adult Dorsal Termini Branching
RFP
50 µm

Adult Δ-*cyc*

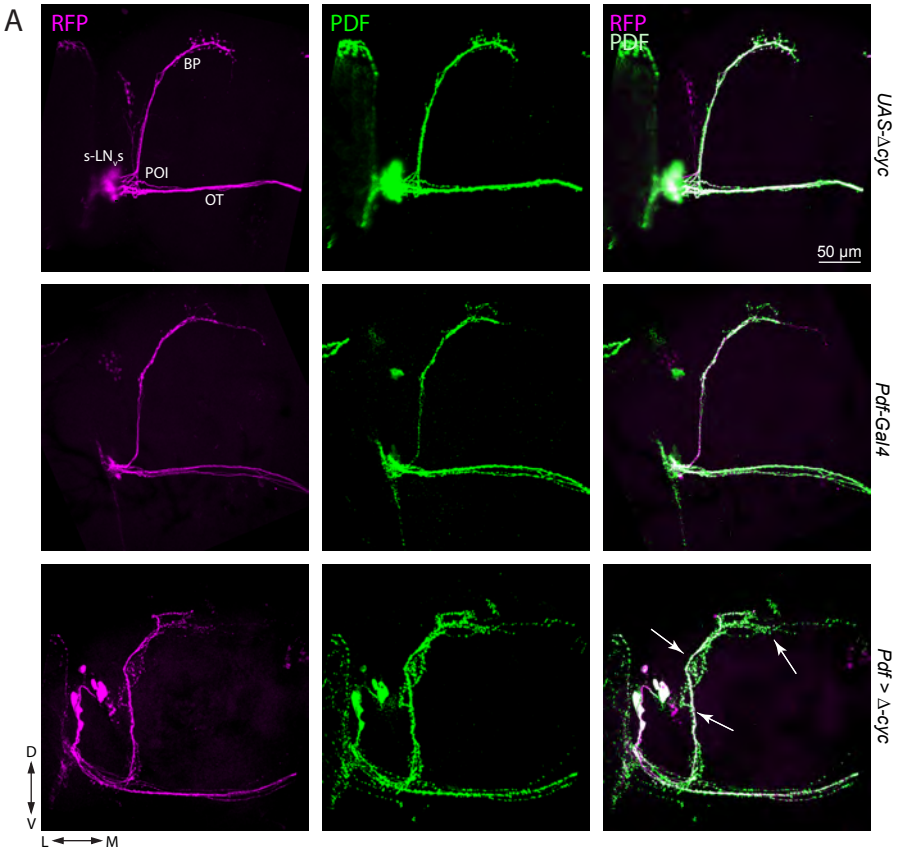
A
RFP
PDF
RFP
PDF
BP
s-LNvs
POI
OT
50 µm
UAS-Δcyc
Pdf-Gal4
Pdf > Δ-cyc
D
V
L
M

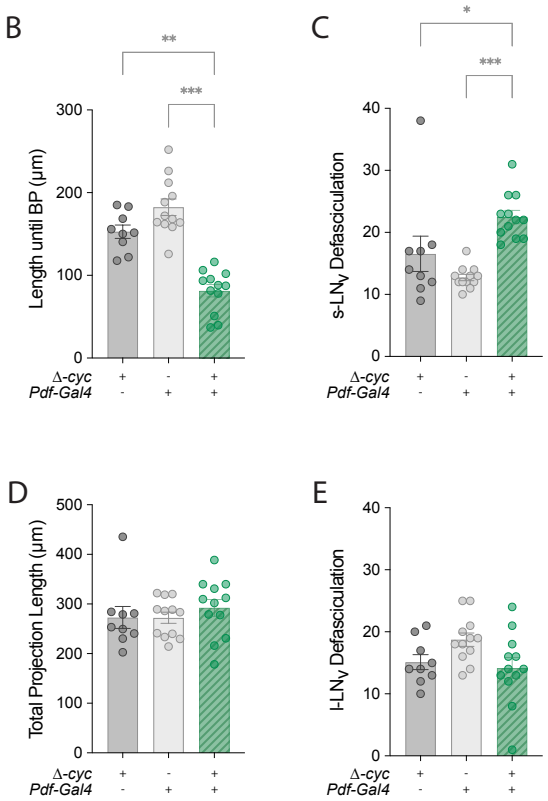
B
Length until BP (µm)
300
200
100
0
**
***
Δ-cyc + - +
Pdf-Gal4 - + +
C
s-LNv Defasciculation
40
30
20
10
0
*
***
Δ-cyc + - +
Pdf-Gal4 - + +
D
Total Projection Length (µm)
500
400
300
200
100
0
Δ-cyc + - +
Pdf-Gal4 - + +
E
l-LNv Defasciculation
40
30
20
10
0
Δ-cyc + - +
Pdf-Gal4 - + +

Adult-specific *cyc* silencing

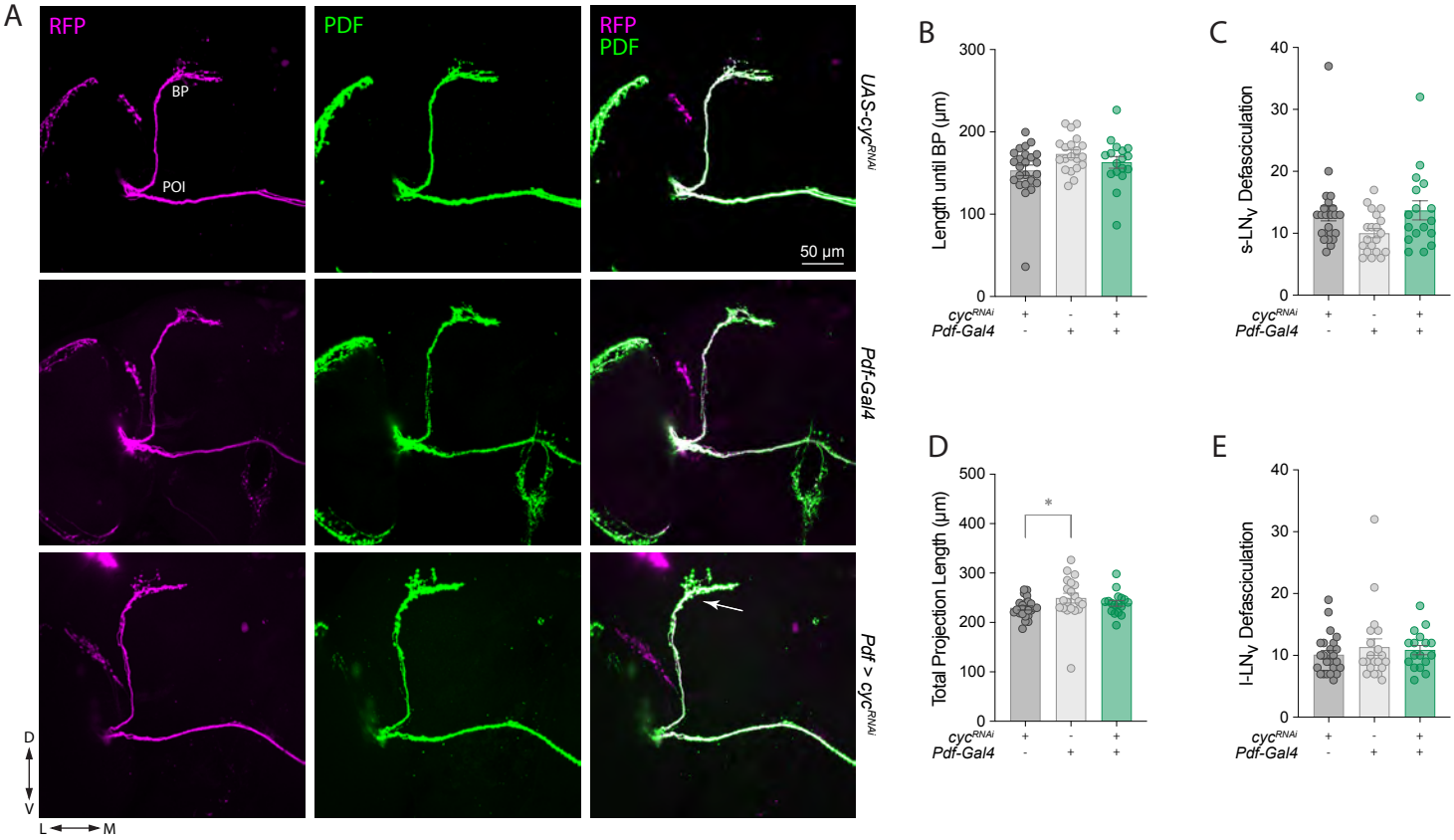

Development-specific *cyc* silencing

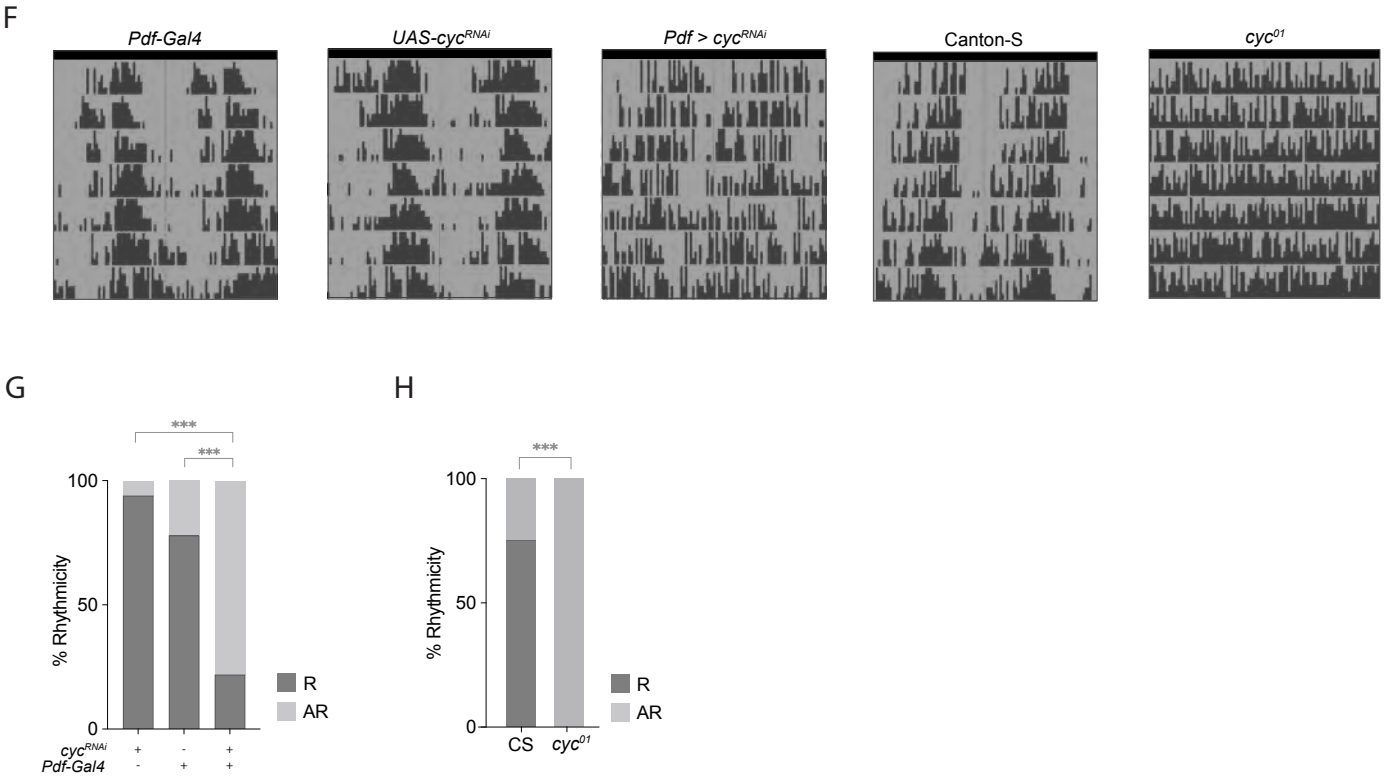

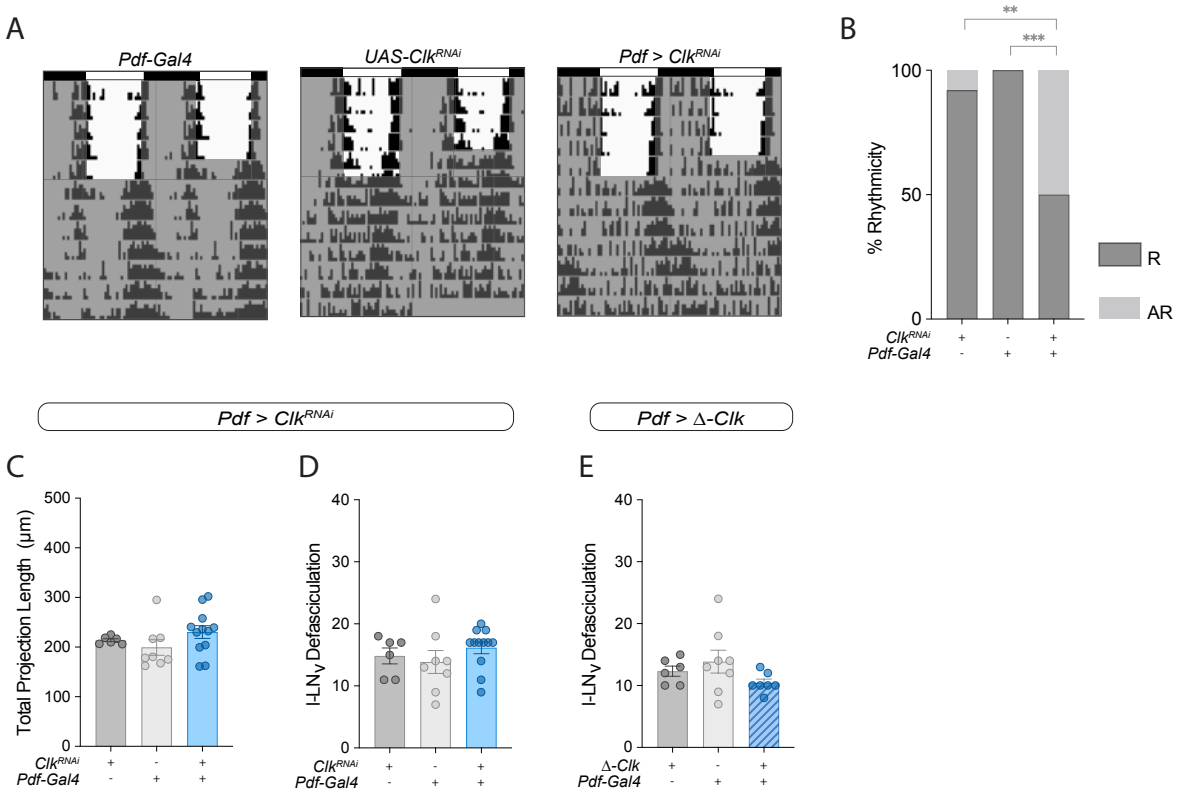
A
Pdf-Gal4
UAS-Clk^RNAi
Pdf > Clk^RNAi
B
**
***
100
50
0
% Rhythmicity
R
AR
Clk^RNAi + - +
Pdf-Gal4 - + +
Pdf > Clk^RNAi
Pdf > Δ-Clk
C
Total Projection Length (µm)
500
400
300
200
100
0
Clk^RNAi + - +
Pdf-Gal4 - + +
D
l-LNv Defasciculation
40
30
20
10
0
Clk^RNAi + - +
Pdf-Gal4 - + +
E
l-LNv Defasciculation
40
30
20
10
0
Δ-Clk + - +
Pdf-Gal4 - + +

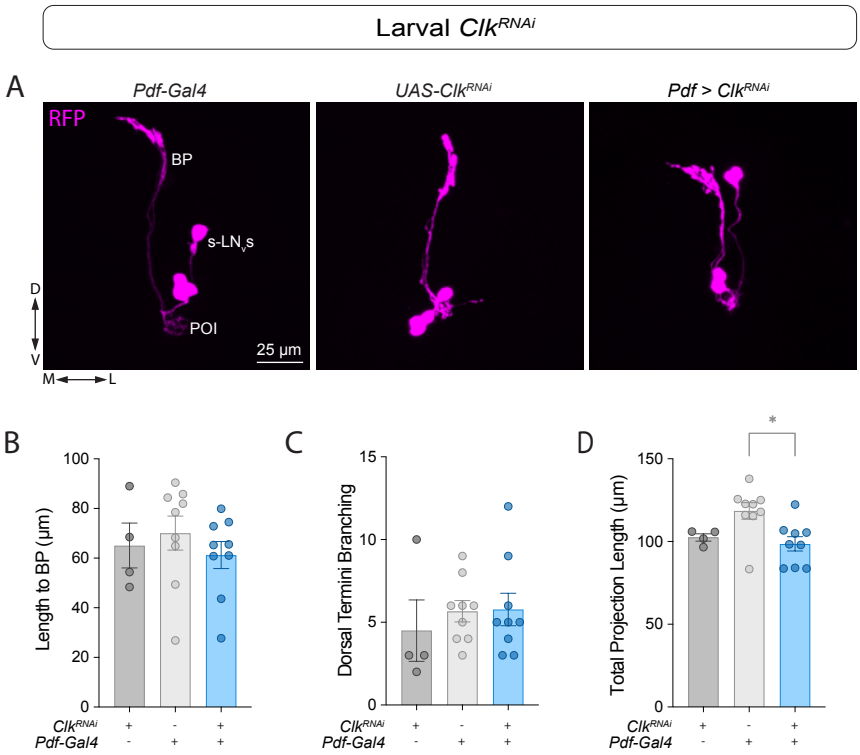
Larval Clk^RNAi
A
Pdf-Gal4
UAS-Clk^RNAi
Pdf > Clk^RNAi
RFP
BP
s-LNvs
POI
25 µm
D
V
M
L
B
Length to BP (µm)
C
Dorsal Termini Branching
D
Total Projection Length (µm)
*
Clk^RNAi
Pdf-Gal4

Table 1. Summary of free running activity rhythms. Related to Figure 2 and Supplementary Figures 3, 4, and 6.

12:12 LD-DD; 28˚C				
Genotype	Number of Flies (n)	% Rhythmicity (nR)	Period (h) ± SEM	Rhythmic Power ± SEM
;Pdf-Red,Pdf-Gal4;Tub-Gal80^{ts}	24	100.00 (24)	24.5 ± 0.06	101.4 ± 8.9
;;UAS-cyc$^{RNAi\ 42563}$	29	75.86 (22)	23.9 ± 0.3	60.5 ± 6.9
;Pdf-Red,Pdf;Tub-Gal80^{ts} > ;;cyc$^{RNAi\ 42563}$	32	6.25 (2)	30.5 ± 3.5	21.69 ± 8.1
;;UAS-Clk$^{RNAi\ 42566}$	26	92.31 (24)	23.8 ± 0.1	93.6 ± 9.4
;Pdf-Red,Pdf;Tub-Gal80^{ts} > ;;Clk$^{RNAi\ 42566}$	26	50.00 (13)	25.4 ± 0.2	40.0 ± 6.5

12:12 LD-DD; 18˚C				
Genotype	Number of Flies (n)	% Rhythmicity (nR)	Period (h) ± SEM	Rhythmic Power ± SEM
;Pdf-Red,Pdf-Gal4;Tub-Gal80^{ts}	27	78 (21)	24.2 ± 0.1	71.5 ± 8.5
;;UAS-cyc$^{RNAi\ 42563}$	32	94 (30)	24.3 ± 0.06	75.6 ± 8.7
;Pdf-Red,Pdf;Tub-Gal80^{ts} > ;;cyc$^{RNAi\ 42563}$	32	22 (7)	22.2 ± 0.2	21.6 ± 3.8
cyc^{01}	14	0	NR	NR

Activity analysis of the above genotypes at either 28˚C or 18˚C. For each genotype, the number of flies (n) is listed above. All flies were raised at 28˚C and then, upon eclosion, kept at 28˚C or transferred to 18˚C. ClockLab's χ-square periodogram analysis was used to analyze rhythmicity, rhythmic power, and free-running period for each above genotypes. The % rhythmicity along with the number of rhythmic flies (nR), the period in hours with the SEM, and the rhythmic power with the SEM are indicated. Arrhythmic flies were not considered in the analysis of period or rhythmic power.